Carbon isotope stratigraphy and depositional oxia through Cenomanian/Turonian boundary sequences (Upper Cretaceous) in New Zealand

Carbon isotope stratigraphy and depositional oxia through Cenomanian/Turonian boundary sequences (Upper Cretaceous) in New Zealand

Takashi Hasegawa [a, *], James Crampton [b], Poul Schiøler [b], Brad Field [b], Keisuke Fukushi [c], Yoshihiro Kakizaki [a, d]

[a] *Department of Earth Sciences, Faculty of Natural Systems, Institute of Science and Engineering, Kanazawa University, Kanazawa 920-1192 Japan*

[b] *GNS Science, P.O. Box 30368, Lower Hutt, New Zealand*

[c] *Institute of Nature and Environmental Technology, Kanazawa University, Kanazawa 920-1192 Japan*

[d] *Present address: Graduate School of Social and Cultural Studies, Kyushu University, Nishi-ku, Fukuoka 819-0395 Japan*

[*]Corresponding author

E-mail addresses: jh7ujr@staff.kanazawa-u.ac.jp (T. Hashegawa); j.crampton@gns.cri.nz (J. Crampton)

ABSTRACT

Stratigraphic sections across the Cenomanian/Turonian boundary (C/T boundary) are identified in New Zealand and were deposited in southern high latitudes of the palaeo-Pacific. Lithological evidence for Cretaceous Oceanic Anoxic Event 2 (OAE2), which preceded and spanned the C/T boundary, is lacking in these sections. The correlative interval is identified, however, from a positive 2‰ carbon isotope excursion (CIE) and from clustered highest occurrences of Cenomanian-restricted dinoflagellate taxa together with the lowest occurrence of Turonian *Heterosphaeridium difficile*. A zone lacking benthic macrofossils encompasses the CIE. In some sections, this interval is also characterized by distinctive red mudstone beds; the thickest such red bed (6–18 m thick) may overlap or just overlie the main part of the CIE interval. Shelly macrobenthos, notably inoceramid bivalves, disappeared >500 kyr prior to the CIE. This suggests that environmental deterioration associated with OAE2 may have preceded the inferred volcanic trigger that has been identified from other regions. Strong intermediate water depth oxia during OAE2, which contrasts with oceanic anoxic conditions that occurred elsewhere on the globe, apparently prevailed during the later phase of OAE2 in the southernmost Pacific. New data from New Zealand indicate that causal mechanism(s) of OAE2 may be complex.

Key words: Oceanic anoxic event, OAE2, Carbon isotope, Cenomanian, Turonian, Cretaceous, Inoceramid, Dinoflagellate, Red bed, New Zealand

1. **Introduction**

Cretaceous oceanic anoxic events (OAEs) are well known geological events that resulted in widespread deposition of organic-rich marine sediments (Schlanger and Jenkyns, 1976), most typically in pelagic carbonate sequences (e.g., Arthur and Premoli Silva, 1982; Arthur et al., 1987; Schlanger et al., 1987). OAE2 at the end of the Cenomanian (93.6 Ma; Ogg et al., 2008; 93.9 Ma; Meyers et al., 2012) is one of the most intensively studied such intervals because of its association with a large perturbation of the carbon cycle (Arthur et al., 1988) and its proximity in time to the Cretaceous thermal maximum (e.g., Clarke and Jenkyns, 1999; Poulsen et al., 2003). It has, in addition, been considered to mark a second-tier global extinction event (e.g., Sepkoski and Raup, 1986; Barnes et al., 1995; Harries and Little, 1999; but cf. Smith et al., 2001). Spatial and temporal patterns of palaeoceanographic change across the OAE2 horizon, based on microfossil palaeontology (e.g., Parente et al., 2008; Pearce et al., 2009; Linnert et al., 2010), stable isotopes (e.g., Ohkouchi et al., 1999; Jenkyns et al., 2007; Forster et al., 2008) and other geochemical proxies (e.g., Kolonic et al., 2005; Forster et al., 2007; Mort et al., 2007; van Bentum et al., 2009; Jarvis et al., 2011) have revealed photic zone euxinia and transient mid-term cooling ("Plenus Cold Event") in the Tethyan and proto-North Atlantic regions during deposition of the sediments. Recently, metal concentration and osmium and lead isotope data have suggested that massive volcanic eruptions associated with large igneous province formation (Snow et al., 2005; Kuroda et al., 2007; Turgeon and Creaser, 2008) may have triggered the climatic and oceanographic changes that occurred during OAE2 (Barclay et al., 2010).

Most studies to date have been based on pelagic strata from Tethyan or Atlantic regions. Even though the Pacific was the largest ocean on Earth during the Cretaceous Period, no continuous OAE2-correlative horizons have been studied except for a small number of clastic successions in Japan (Hasegawa, 1997; Nemoto and Hasegawa, 2011). Despite the obvious interest, no complete sections through OAE2 have been identified or described from the South Pacific region. In particular, although mid-Cretaceous clastic successions are known from New Zealand (e.g., Crampton et al., 2001), the Cenomanian/Turonian boundary has never been located confidently or precisely. This reflects both the endemic nature of many New Zealand fossil species and the consequent difficulty of correlating New Zealand stages to the international time-scale (Cooper 2004), and the lack of obvious sedimentary expression of OAE2 in any studied sections (e.g., Hikuroa et al., 2009). Here, we present new data on lithology, biostratigraphy and carbon isotope stratigraphy through four New Zealand on-shore sections that potentially include the Cenomanian/Turonian boundary, and we locate OAE2-correlative intervals in three of these sections.

Our goals are three-fold. First and foremost, the results presented here are important for inter-regional correlation and timescale development. Secondly, we hope to provide data that will begin to elucidate palaeoceanographic and palaeoclimatic responses in the southernmost

Pacific to OAE2. During the mid-Cretaceous, New Zealand lay at a palaeolatitude of about 70ºS (Sutherland, 1999) and our observations are consistent with the presence of oxygenated intermediate-depth water in southern high latitudes of the Pacific Ocean during the period of OAE2 (cf. Hay et al., 1999; Otto-Bliesner et al., 2002; Hay, 2009;). Lastly, although Cretaceous black shales have not been identified in the New Zealand region, hydrocarbon generation modelling of the East Coast Basin of the North Island indicates that there could have been hydrocarbon generation from mid-Cretaceous source rocks (Field and Uruski, 1997). This inference is consistent with the presence of thermogenic gas seeps in localities where latest Cretaceous and younger source rocks are modelled as immature for gas generation (Field and Uruski, 1997), and with the presence of an oil seep on Raukumara Peninsula that may be derived from mid-Cretaceous rocks (Killops, 1996). The East Coast Basin appears to have a viable petroleum system and, although it is still regarded as a frontier region, most of the area is under licence to active hydrocarbon exploration companies. Our third aim, therefore, is to help constrain the likely position and expression, if any, of OAE2 in the New Zealand stratigraphic record.

All samples discussed here are housed at GNS Science, Lower Hutt, New Zealand; geochemical samples are assigned “P” (petrological) numbers within the relevant topographical map sheet and are catalogued within the PETLAB Database (http://pet.gns.cri.nz/index.jsp); palaeontological samples are assigned “f” (fossil) numbers and are catalogued by relevant topographical map sheet within the Fossil Record File Database (http://www.fred.org.nz/index.jsp). Outcrop photographs with sample localities marked (indexed using field sample numbers, see Tables 1, 2) can be downloaded from the Fossil Record File.

2. Geology and setting

The Cenomanian/Turonian boundary is inferred to lie within the upper part of the Arowhanan Stage of the New Zealand geological timescale (Cooper, 2004; Hollis et al., 2010). Marine siliciclastic strata of Arowhanan age are distributed widely throughout the East Coast Basin (sensu Field and Uruski, 1997), from Marlborough (northeastern South Island) to the Raukumara Peninsula (eastern North Island; Fig. 1). In addition, they occur within structurally complex sequences in Northland (Isaac et al., 1994). All four sections studied here lie within the East Coast Basin; from north to south, they are the Mangaotane A and B, Glenburn and Sawpit Gully sections (comprising adjacent, partially overlapping northern and southern sections).

2.1. Mangaotane A section

Mangaotane Stream is a tributary of the Motu River, and it drains the southern part of the Raukumara Range, Raukumara Peninsula, approximately 60 km north-northwest of Gisborne (Fig. 1). The section exposed over several kilometers of this stream was identified by Wellman (1959) as the interval stratotype for the Arowhanan, Mangaotanean and Teratan New Zealand stages. Subsequently, revised lower boundary stratotypes of all three stages have been designated in the stream (Crampton et al., 2001; Cooper, 2004). Previous descriptions of the locality are listed in Crampton et al. (2001), and a general introduction to the geology of the Raukumara Peninsula is given in Mazengarb and Speden (2000).

The interval studied here extends over 255 m stratigraphically and is exposed continuously in both banks of Mangaotane Stream along an east-northeast-flowing leg at a prominent “Z-bend” (Fig. 2). The base of the section is at grid reference NZ Topo50 BE42 (Houpoto) 19306877 (± 5 m); the top of the section is at BE42 19156864 [NZMS 260 map series, sheet X16 (Motu), 29273012 (± 5 m) to X16 29122999]. An east-west-trending fault cuts across the stream and there is some uncertainty in correlation across this fault and the stream, although there does not appear to be very significant omission or repetition of section across this structure, based on both macro- and microfossil correlations. The section was sampled for the present study in April 2002, November 2005 and March 2009. The three sample suites were integrated in the field using comprehensive outcrop photographs taken during each of the earlier sampling campaigns. In a few cases, significant changes in the appearance of outcrops between 2002 and 2005 prevented precise correlation of sample sites (indicated on Fig. 3), although errors are likely to be small (< 1 m).

The oldest strata in the section comprise overturned, indurated, centimetre- to decimetre-interbedded, mudstone and very fine sandstone of the Waitahaia Formation (Fig. 3); the proportion of sandstone decreases up-section from ~30% to <5%. Overlying this with gradational contact, the Karekare Formation is composed of steeply to moderately dipping, indurated mudstone and minor, millimetre- to 5 cm-bedded, very fine sandstone. A conspicuous feature of the section is the presence of several reddish-brown (Munsell colour dusky brown, 5 YR 3/2) mudstone beds in the Karekare Formation; in places these beds are associated with pale greenish-weathering intervals. The thickest of these "red" beds, at ~225 m in the section, is ~6 m thick (Fig. 3), although this is unlikely to be the true value because of poorly constrained effects of numerous minor faults and shears. Aspects of the geochemistry of the red beds have been described by Hikuroa et al. (2009). These red beds may have been deposited, in part, by low density turbidity currents (Hikuroa et al., 2009), although the relative importance of deposition by density currents versus from hemipelagic fallout is unknown. As such, it is uncertain whether they should be regarded, strictly, as Cretaceous oceanic red beds (CORBs) sensu Hu et al. (2009, and references therein). Despite this, as shown below, red mudstone beds in the Mangaotane sections almost certainly have some genetic similarities to geographically widespread, typical, pelagic, early Turonian CORBs described from the Tethys and elsewhere (Hu et al., 2009).

Inoceramid bivalve fossils are abundant through most of the Karekare Formation, and particularly so in the interval between ~90 and ~200 m, and above ~235 m. Other fossil groups have not been observed in the section. A conspicuous interval that is barren of inoceramids occurs between ~209 and 235 m, at about the level of the thick red bed (barren interval indicated on Fig. 3). We stress that repeated and detailed sampling of this section over many years, by several geologists, has failed to locate any macrofossils within this barren interval. The section studied spans most of the *Magadiceramus rangatira haroldi* Zone and all of the overlying *M. rangatira rangatira* Zone, which together comprise the Arowhanan Stage, and the lowest part of the *Cremnoceramus bicorrugatus matamuus* Zone of the Mangaotanean Stage (inoceramid bivalve zones described in Crampton, 1996, and shown on Fig. 3). Inoceramid biostratigraphy of the Mangaotane A section has been described in detail by Crampton et al. (2001). From sparse foraminiferal assemblages and comparatively rich dinoflagellate floras, it seems likely that these rocks were deposited in a restricted, bathyal or deeper marine environment, remote from land, with variable, poor to moderate circulation (Crampton et al., 2001).

2.2. Mangaotane B section

This section lies on the eastern limb of a conspicuous horse-shoe bend in Mangaotane Stream, just over 2 km northwest and downstream of the Mangaotane A locality (Fig. 2). The base of the section is at grid reference NZ Topo50 BE42 (Houpoto) 17607038 (± 5 m); the top of the section is at BE42 17567024 [NZMS 260 map series, sheet X16 (Motu), 27583173 (± 5 m) to X16 27543159]. The section was logged and sampled in March 2009. Approximately 40 m of moderately to gently dipping strata were recorded from both banks of the stream. These strata span just the major, thick red bed seen in the Mangaotane A section; in the Mangaotane B section this bed is very well exposed, is not significantly affected by faulting, and is ~18 m thick (Figs. 4, 5). In most other respects, strata exposed at the Mangaotane B locality resemble correlative strata in the Mangaotane A section. Apart from abundant specimens of *M. rangatira rangatira* that occur at the very base of the Mangaotane B section (indicated on Fig. 4), macrofossils are apparently absent from this section and we infer that the logged interval correlates with the macrofossil barren zone observed in the Mangaotane A section.

2.3. Glenburn section

The Glenburn section is at Glenburn on the Wairarapa coastline, approximately 90 km east of Wellington (Figs. 1, 6). The base of the section is at grid reference NZ Topo50 BQ35 (Te Wharau) 38092084 (± 5 m); the top of the section is at BQ35 38152084 [NZMS 260 map series, sheet T27 (Te Wharau), 48118257 (± 5 m) to T27 48178257]. The section occupies a shore platform on the south side of Horewai Point, exposes steeply dipping Glenburn Formation, and was logged originally by Crampton (1996, fig. 19; 1997, fig. 25). The geology of the area is structurally complex and has been described, in general terms, by Lee and Begg (2002). In March 2009, for the present study, we re-logged in detail a section 75 m thick that spans the boundary between the *M. rangatira haroldi* inoceramid Zone and *M. rangatira rangatira* Zone; the base of this log is at the top of a conglomerate bed at 65 m on the section of Crampton (1997).

Over the logged interval, the Glenburn Formation comprises indurated, mudstone-dominated, decimetre- to centimetre-interbedded, alternating sandstone and mudstone, with minor conglomerate beds at the base (Fig. 7). Inoceramid bivalves are abundant throughout the section; the inoceramid biostratigraphy has been described by Crampton (1996). Based on sedimentological characteristics and preliminary palynofacies interpretations, the Glenburn Formation at Glenburn is inferred to represent a relatively deep-water facies that was deposited by gravity flow processes (mainly turbidites) at bathyal or greater depths.

2.4. Sawpit Gully sections

These two closely-spaced sections lie in the lower reaches of “Sawpit Gully” (informal name), a small tributary of Nidd Stream on the southeastern flanks of the Chalk Range, close to Coverham at the northern end of the Clarence River valley and about 50 km south of Blenheim, in Marlborough (Figs. 1, 8). The base of the section is at grid reference NZ Topo50 BS28 (Kekerengu) 72595651 (± 5 m); the top of the section is at BS28 72665665 [NZMS 260 map series, sheet P30 (Clarence), 82611819 (± 5 m) to P30 82681834]. The geology of the Coverham area is extremely complex, both stratigraphically and structurally; a generalized geological map of the area is given in Rattenbury et al. (2006), a more detailed map of the Coverham area was provided by Crampton et al. (1998, fig. 6; 2004, fig. 3), and Cretaceous palaeogeographic maps of eastern Marlborough are given in Crampton et al. (2003). As part of the present study, the locality was sampled in November 2005, March 2009, and March 2010; the sample suites were integrated at the time of sampling using comprehensive outcrop photographs taken during each of the earlier field seasons. The section shown here (Fig. 9) is in two parts, the southern and northern sections. The lower part is exposed within the stream bed and both banks, and across the southern limb of a syncline in a large eroding face on the eastern side of the stream. The upper and partially overlapping section is exposed on the northern limb of the same syncline. Although the two sections cannot be correlated precisely because of structural thickening in the syncline, the correlation shown in Fig. 9 is based on tracing of individual beds through the core of the syncline at the top of the outcrop and is likely to be correct to within a few metres.

Taken together, the sections expose ~120 m of moderately indurated, concretionary siltstone, silty sandstone, and sandstone of the Nidd Formation. They span the upper part of the *M. rangatira rangatira* Zone, all of the *C. bicorrugatus matamuus* Zone, and the lower part of the *C. bicorrugatus bicorrugatus* Zone (Fig. 9). Inoceramid bivalves are common low in the succession, below 54 m in the southern section. They are very abundant in the upper part of the succession, above ~19 m in the northern section (Fig. 9). Between these two levels macrofossils are apparently lacking. As in the Mangaotane A section, repeated sampling over many years has failed to discover macrofossils within this barren interval. Small inoceramids collected from the ~10 m of section overlying the barren interval in the northern section cannot be identified to species level and the zone and stage assignment of these strata remains uncertain (Fig. 9). The environment of deposition of Nidd Formation is poorly constrained, but palaeontological and sedimentological interpretations, and the stratigraphic context, suggest that it was likely to have been deposited at mid- to outer shelf depths.

3. Methods

3.1. Rock-Eval pyrolysis

Rock-Eval pyrolysis was carried out on 15 samples from Mangaotane A, six from Glenburn and five from Sawpit Gully sections, and the hydrogen Index (HI), T_{max} and whole rock-based total organic carbon content (TOC) were determined. Powdered mudstone samples were processed and analyzed according to standard techniques (Espitalie et al., 1985). These analyses were undertaken at the organic petrology and geochemistry laboratory of the Geological Survey of Canada. Based on re-analysis of standards, relative errors on TOC measurements determined by Rock-Eval pyrolysis are assumed to be smaller than ±5%.

3.2. Carbon isotope and total organic carbon (carbonate-free basis) analyses

For the Mangaotane A section, 72 geochemical samples were analyzed. Samples were cut dry on a diamond saw to isolate an untouched block that was then wrapped in aluminum foil that had been pre-heated to 500ºC to destroy any organic contaminants; gloves were used throughout to avoid further contamination. The dry blocks were crushed to <1 mm chips using a press or clean hammer. A sample splitter was used to yield a fraction of at least 4 g. A single fraction per sample was ground finely and used for both isotopic and Rock-Eval analyses.

About 40 mg of each sample from the Mangaotane A section was powdered using a mortar and pestle and reacted with 1 M HCl for eight hours to remove carbonate, then washed with de-ionized water to neutralize, and dried. Samples were first run on a Europa ANCA elemental analyser connected to a PDZ Europa Geo 20-20 mass spectrometer in continuous flow, following combustion in the presence of excess oxygen at 1100ºC, to obtain preliminary carbon isotope ratio ($\delta^{13}C$) and carbonate-free basis total organic carbon content (TOC_{cf}). In duplicate, another 40 mg was put in glass tubing with CuO, sealed under evacuation then heated at 850ºC for 8 hours to convert organic carbon into CO_2. The CO_2 was then purified through a cryogenic vacuum line and was run on a PDZ Europa Geo 20-20 mass spectrometer using dual inlet system. Both these sets of analyses were undertaken at the Rafter Stable Isotope Laboratory, GNS Science, New Zealand. Each isotopic value reported herein is the result of dual inlet analysis and is normalized to internationally accepted scales, Vienna PeeDee Belemnite (VPDB) for carbon, based on the ratio of heavy to light isotopes in the sample (Rs) relative to the standard (Rstd): $\delta^{13}C$ (‰) = (Rs–Rstd)/Rstd × 1000. The results are calibrated by NBS22 and ANU-sucrose standards. The standard deviation for each analysis is smaller than 0.1‰. The TOC_{cf} of each sample was calculated from the peak area of the mass chromatograms; relative errors on TOC_{cf} measurements are smaller than ±5%.

Geochemical samples from the Mangaotane B and Glenburn sections and samples from the Sawpit Gully section taken in 2009 were analysed as follows. Approximately 1 g of powder was obtained from fresh surfaces of each rock sample using a dental grinder. About half of the powder for isotope analysis was treated in glass tubes with 5 N HCl for eight hours to remove carbonate, then washed with de-ionized water to neutralize, and dried. An approximately 10–60 mg subsample was extracted from each neutralized sample, placed in a tin film cup and weighed. These samples were introduced into a SerCon elemental analyzer (EA) ANCA, combusted at 1000ºC, and the sample-derived CO_2 was transferred into an EA-connected SerCon 20-20 mass spectrometer for $\delta^{13}C$ analyses. Samples from Sawpit Gully section collected in 2010 were processed in the same manner as the 2009 samples, but analyzed with a Thermo Electron Delta V mass spectrometer equipped with NA2500 EA with combustion temperature of 1000ºC. These analyses were undertaken at Kanazawa University, Japan. The $\delta^{13}C$ results reported herein were obtained using reference CO_2 produced from a single bottle of L-alanine provided by Shoko Tsusho Co. Ltd. that is calibrated by ANU-sucrose directly and NBS-19 indirectly. Each data point is an average of triplicate analyses for each sample and is expressed in the δ notation as described above. Repeated analysis of a laboratory standard indicates ±0.2‰ as the instrumental reproducibility for a single analysis. As above, the TOC_{cf} of each sample was calculated from the peak area of the mass chromatograms; relative errors on TOC_{cf} measurements are smaller than ±5%.

Inter-laboratory calibration for $\delta^{13}C$ values, between GNS Science and Kanazawa University, was accomplished using two different laboratory standards (leucine: -22.7‰; flour: -27.3‰) and three internationally distributed standards, namely ANU-Sucrose (-10.45‰), IAEA2711 (-17.1‰) and NIST8704 (-19.8‰).

Full results of the carbon isotope, TOC_{cf} and Rock Eval analyses are given in the Supplementary data.

3.3. Organic petrology

Organic compositions of mudstone samples collected from the Mangaotane A section for carbon-isotope analysis were checked by visual observation of kerogen in order to identify organic particles. Seventeen samples, including two samples from outside the range of the section described here [P77167 (~ -25 m), P77169, P77172, P77179, P77186, P77194, P77198, P77199, P77201, P77208, P77218, P77228, P77231, P77234, P77235, P77238, P77242 (271 m)], were crushed and made into polished blocks following standard preparation procedure (Bustin et al., 1983). Polished pellets were examined under reflected (white) light and transmitted (fluorescent mode) light using a microscope equipped with an oil-immersion objective.

3.4. Dinoflagellates

In addition to the geochemical and petrological analyses described above, we examined the dinoflagellate biostratigraphy of the Mangaotane A and Sawpit Gully sections. Fifty-eight samples were studied (Tables 1, 2), spanning both sections. The samples were processed following standard palynological techniques for pre-Quaternary samples (cf. Batten, 1999), including treatment with 5N hydrochloric acid, 40% hydrofluoric acid and two minutes oxidation in 36% nitric acid followed by heavy liquid separation using sodium polytungstate. Treatment with dilute alkali after the oxidation and ultrasonic treatment were not used. The sample residue was filtered on 11 μm filter cloth and mounted in glycerine jelly. The samples were studied qualitatively for dinoflagellates and acritarchs. Dinoflagellate taxa mentioned in the text are fully referenced in the Lentin and Williams index (Fensome et al., 2004).

4. Results

4.1. Rock Eval pyrolysis

All samples on which Rock Eval pyrolyses were carried out have hydrogen indices lower than 50 mg_{HC}/g_{TOC}, whereas their T_{max} values exhibit distinctive bimodal distributions. All T_{max} from the Sawpit Gully and Glenburn sections are concentrated around 435°C. In contrast, data from the Mangaotane A section are distributed widely above 520°C except for a single data point that was collected below the logged interval and is close to measurements from the other sections.

4.2. Organic petrology

Visual observation of kerogens in selected samples from the Mangaotane A section showed that organic matter is largely terrestrial in origin. The bulk of organic matter observed under a microscope is composed of vitrinite (Fig. 11D) and semifusinite (Fig. 11C). Minor non-fluorescent brown amorphous organic matter is not marine in origin but terrestrial (Omura and Hoyanagi, 2004). Liptinite, which is potentially marine algal in origin, is also observed as a minor (<<5% of total organic matter) component (Fig. 11A). Three samples from the thick red bed (P77234, P77235) and a minor red bed (P77198), with very low TOC values, contain much lower amounts of terrestrial kerogen. Semifusinite is substantially lacking from these samples whereas fusinite is more abundant relative to semifusinite and vitrinite (Fig. 11B). In addition, shaped kerogen particles in the red beds are small relative to other samples examined.

4.3. Total organic carbon content (carbonate-free basis; TOC_{cf})

TOC_{cf} through the Mangaotane A section generally shows relatively higher values above 0.3% in the lower part from 0 to 100 m, except for the interval between 50 and 75 m where TOC_{cf} is approximately 0.2% (Fig. 3 left, Fig. 12A). In contrast, the majority of the samples from the upper part of this section show a TOC_{cf} of around 0.2% or slightly lower. A conspicuous drop to <0.1% is observed between 218 and 232 m in the thick red bed (Fig. 3, Fig. 12A). TOC_{cf} lower than 0.1% was also detected in four horizons of the thick red bed in the Mangaotane B section (Fig. 4). TOC_{cf} in samples from the other sections generally show higher values than the Mangaotane sections. All samples from the Glenburn section range between 0.17% and 0.55% (Fig. 7) and those from the Sawpit Gully section range between 0.21% and 0.47% (Fig. 9).

4.4. Carbon isotope stratigraphy

The carbon isotope profile through the Mangaotane A section is characterized by a positive 0.3‰ trend up-section, from ~ -24.6‰ to ~ -24.3‰, and a short-lived 0.5‰ negative excursion near the top, between 220 and 250 m. (Fig. 12B). Superimposed on this trend are two conspicuous, comparatively large, negative 'excursions' in $\delta^{13}C$ within the intervals 56–75 m and 218–230 m. The $\delta^{13}C$ values of the lower negative interval are -25.8‰, -25.9‰ and -26.8‰. The upper negative interval, with values as low as -27.6‰ (P77234), corresponds to the horizon of minimum TOC_{cf} within the thick red bed. This relationship between $\delta^{13}C$ and TOC_{cf} is also observed in the Mangaotane B section. The most positive $\delta^{13}C$ value observed in the Mangaotane A section is -24.0‰ at 220 m (P77229), within distinctive, alternating beds of red and olive-grey mudstones beneath the thick red bed. In the Mangaotane B section, the most positive value, -23.5‰ (X16/f312), was measured within alternating beds of red and olive-grey mudstone lying within the lower part of the main red bed interval, a pattern that appears to be broadly similar to that observed in the Mangaotane A section. The value -23.5‰ is significantly more positive than the general "background" trend in both Mangaotane sections that, as noted above, ranges between -25‰ and -24‰.

The lower part of the southern Sawpit Gully section shows very stable $\delta^{13}C$ of about -25‰ (Fig. 9). The most negative value observed in the section,-25.2‰, at 57.6m (f1649), is overlain by a dramatic positive excursion of about 2‰. The onset of the positive excursion is observed at 59 m (f1603) and the most positive value (-23.16‰) is at 66.5 m (f1642). Above this, $\delta^{13}C$ shows a stepped recovery from -23.2‰ towards -25‰ in the interval between 72.6 and 88.9 m. Complete recovery to the pre-excursion value is observed at 88.6 m (f1646), near the top of the southern section. In the northern Sawpit Gully section, a similar positive excursion is also observed. The excursion is followed by a recovery to -24.8‰ at 18 m (f1618) and, thereafter, approximately stable measurements of ~ -24.5‰. It is notable that all of the peak values in the Mangaotane A, B and Sawpit Gully sections are recorded in the middle of the zone barren of macrofossils that occupies the uppermost part of the *M. rangatira rangatira* Zone.

In contrast to the other sections, $\delta^{13}C$ values from the stratigraphically lower Glenburn section show remarkably stable values of around -24.6‰, with no observed trend or excursions (Fig. 7).

4.5. Dinoflagellate biostratigraphy

Palynological samples from the Mangaotane A and Sawpit Gully sections contain rich but poorly preserved, generally dark-coloured, palynomorph assemblages that are dominated by dinoflagellates. Key dinoflagellates are listed in Tables 1 and 2 and illustrated in Fig. 10, and key dinoflagellate biostratigraphic datums are shown in Figs. 3 and 9. The dinoflagellate assemblages are similar to contemporaneous palynofloras from Australia and Antarctica, but also contain species that may be used to correlate the section with northwest European strata and the Cenomanian/Turonian boundary-stratotype section. The dinoflagellate floras are characterised by long-ranging *Heterosphaeridium* spp., *Odontochitina* spp., *Oligosphaeridium* spp., *Pterodinium* spp., and *Spiniferites* spp., and mid–Late Cretaceous taxa such as *Anthosphaeridium convolvuloides*, *Cyclonephelium* spp., *Cymososphaeridium benmorense*, *Hystrichodinium pulchrum, Hystrichodinium ramoides, Isabelidinium acuminatum*, *Pervosphaeridium pseudhystrichodinium*, *Prolixosphaeridium conulum* and *Sepispinula ambigua*.

The distribution of a small number of key dinoflagellates may be used, however, to constrain further the age of the two sections and strongly supports a Cenomanian age interpretation for the lower two thirds of the Mangaotane A section and the lower half of the southern Sawpit Gully section (Fig. 10). In particular, the highest occurrences (HO) of *Ascodinium serratum* at 83.7 m and *Hapsocysta peridictya*, at 212.7 m in the Mangaotane A section are recorded at the top of the *Endoceratium ludbrookiae* Zone of Morgan (1980). This zone corresponds to the *Diconodinium multispinum* Zone of Helby et al. (1987) that, according to Partridge (2006), spans all of the Cenomanian in Australia. The top of *A. serratum* is probably below the base of the Sawpit Gully section, but *H. peridictya* has an HO at 54.1 m in that section. The HO of *Ascodinium parvum* is recorded at 181.9 m in the Mangaotane A section and at 10.5 m in the southern Sawpit Gully section and lies within the top of the *D. multispinum* Zone.

The HO of *Lithosphaeridium siphoniphorum glabrum* is a palynological proxy for the C/T boundary at its type section (Dodsworth, 2000; Kennedy et al., 2005) and is correlated with this boundary in southern UK and northern Germany (Dodsworth, 2000; Pearce et al., 2009). This event is also located at the top of the Cenomanian *D. multispinum* Zone in the zonation of Helby et al. (1987). The HO of *L. s. glabrum* is at 181.9 m in the Mangaotane A section and at 54.1 m in the southern Sawpit Gully section. The HO of *Kiokansium unituberculatum* has not been reported widely in Australasia, but occurs at the top of the Cenomanian on the Scotian Margin, Canada (Fensome et al., 2009) and in northwest Europe (Costa and Davey, 1992). Its location at 204.4 m in the Mangaotane A section and at 54.1 m in the southern Sawpit Gully section may indicate a Cenomanian age up to those levels. *Eurydinium saxoniense* has been reported widely from a narrow interval around the C/T boundary in Europe (e.g., Marshall and Batten, 1988; Hart et al., 1993; Fitzpatrick, 1995; Dodsworth, 2004) and in Colorado, USA (Courtinat, 1993). This taxon was recorded in the interval 207.6–244 m (top of section) in the Mangaotane A section and from 69.1 m in the southern Sawpit Gully section to 111.9 m in the northern Sawpit Gully section, indicating proximity to the C/T boundary.

The lowest occurrence (LO) of *Heterosphaeridium difficile* at 224.1 m in the Mangaotane A section, and its presence in the two uppermost samples studied herein (237 and 244 m), indicates a Turonian age for the topmost part of the section (Fitzpatrick, 1995; Dodsworth, 2000; Pearce et al., 2003). The LO of *H. difficile* occurs in the lowest sample examined in the northern Sawpit Gully section, and it may extend as low as 69.1 m in the southern Sawpit Gully section (as *H.* cf. *difficile*).

In summary, the clustering of highest occurrences of taxa restricted to Cenomanian and older strata in the interval 181.9–212.7 m in the Mangaotane A section and between 10.5 and 54.1 m in the southern Sawpit Gully section indicates a Cenomanian age for levels below 212.7 m in the Mangaotane A section and below 54.1 m in the Sawpit Gully section. The LO of *H. difficile* at 224.1 m in the Mangaotane A section, immediately below the thick red bed, argues for a Turonian age at and above this level. The sample at 217.5 m is barren of dinoflagellates. Hence, the C/T boundary may be placed between 212.7 and 224.1 m, based on dinoflagellate biostratigraphy. Using the same argument, the C/T boundary may be placed between 54.1 and ?69.1 m in the southern Sawpit Gully section, and below 7.7 m in the northern Sawpit Gully section.

5. Discussion

5.1. Origin of organic matter: What do the $\delta^{13}C$ curves mean?

The inferred origin of organic material provides important clues to the interpretation of $\delta^{13}C$ analyzed with the bulk combustion method. A cross-plot of hydrogen index (HI) versus T_{max} (Fig. 13) shows the results of Rock Eval pyrolysis on selected samples from the Mangaotane, Glenburn, and Sawpit Gully sections. All of the data plot within the region of type III/IV kerogen and the majority of the kerogens are interpreted to be terrestrial in origin (Espitalie et al., 1985; Tyson, 1995). Mudstone samples with comparable organic characteristics from Hokkaido were studied by Hasegawa (2001). There the kerogens are exclusively terrestrial in origin and lie within the oil-generative maturity window, based on organic petrological analysis. Bulk carbon isotope stratigraphies for the Hokkaido sections (Hasegawa and Saito, 1993; Hasegawa, 1997; Uramoto et al., 2009; Hasegawa et al., 2010) are readily correlated to international reference sections (Jarvis et al., 2006), indicating that they reflect C-isotopic fluctuation of the ocean-atmospheric CO_2 reservoir. Since the organic characteristics of samples from the Sawpit Gully and Glenburn sections are almost identical to those from Hokkaido (Fig. 13), the $\delta^{13}C$ stratigraphies of these New Zealand sections are inferred to be meaningful for international correlation.

In contrast, higher T_{max} and lower HI values of samples from the Mangaotane A section may suggest significant oxidation during transport to the depositional site (Tyson, 1995). Alternatively, organic matter in the Mangaotane sections may have experienced greater heating into the dry gas phase. $\delta^{13}C$ values of samples from the *M. rangatira haroldi* (*Mrh*)/*M. rangatira rangatira* (*Mrr*) zone-boundary interval (P77189–77206) in the Mangaotane A section are relatively uniform, lying between -24.61 and -24.10‰, and comparable to correlative samples from the Glenburn section. This observation suggests that the Mangaotane samples essentially retain the original record of $\delta^{13}C$ and reflect secular variation of the ocean-atmosphere reservoir.

Interpretation of $\delta^{13}C$ in other intervals of the Mangaotane A and B sections is more difficult and negative excursions are best explained by changes in the composition of organic matter. Across the main thick red bed, sharp negative spikes of $\delta^{13}C$ values are correlated with drops in TOC (Figs. 3, 4, 12). Microscopic examination of samples P77234 and P77235 (Mangaotane A section) reveals that terrestrial kerogens, namely vitrinite and inertinite, are largely absent within the red bed. In this case, low TOC and/or the oxidized nature of organic matter make it difficult to interpret the Rock Eval result (P77235). The majority of Mangaotane samples contain a minor amount of exinite derived from marine plankton (Fig. 11A). Taken together, these observations suggest that a significant decrease of organic supply from terrestrial plants reduced the total concentration of organic material in the sediments at this level and resulted in a relatively higher contribution of marine organic matter. As marine organic material from Cenomanian–Turonian sequences is known to be 2 to 4‰ more negative than coeval terrestrial organic matter (Pratt and Threlkeld, 1984; Kuhnt et al., 1990; Hasegawa, 1997; Nemoto and Hasegawa, 2011), compositional changes in the source of organic matter can therefore explain the negative $\delta^{13}C$ spikes in and around the red beds near the top of the Mangaotane A section and in the Mangaotane B section. We note that negative excursions in $\delta^{13}C$ have been recorded in a number of Cretaceous carbonate-dominated oceanic red beds, probably related to changing productivity and ratios of organic to inorganic carbon (Hu et al., 2009, and references therein).

Samples P77181, 77184, and 77185 from between 57 and 75 m in the Mangaotane A section show negative $\delta^{13}C$ values of between -25.7 and -26.8‰ and may also be caused by relatively higher contributions from marine organic matter. These fluctuations, however, do not co-vary with TOC_{cf} and further analysis is required to understand isotopic values within this interval. In general, and with the exception of these samples, patterns of $\delta^{13}C$ fluctuation described here for the Mangaotane A section were reproduced by both dual inlet and EA-combustion isotopic analyses.

5.2. Previously estimated Cenomanian/Turonian boundary sequences

Based on general biostratigraphic considerations and preliminary carbon isotopic data from the Mangaotane A section, the Cenomanian/Turonian (C/T) boundary was previously correlated approximately with the *Magadiceramus rangitira haroldi*/*Magadiceramus rangitira rangitira* (*Mrh/Mrr*) zonal boundary, where three distinct, thin (<0.6 m thick) red beds are observed (Crampton et al., 2001; Hikuroa et al., 2009). New carbon isotope stratigraphic results, however, reveal a stable pattern and no positive excursion through this interval, a finding that has been replicated from both the Mangaotane A (Fig. 3) and Glenburn sections (Fig. 7), based on analyses from separate laboratories. The relatively uniform pattern of $\delta^{13}C$ values through this interval indicates that the *Mrh/Mrr* boundary is not correlated with the C/T boundary. Instead, it appears to lie within the middle–upper Cenomanian stable segment that has been observed in carbonate carbon in European sections (Jarvis et al., 2006) and terrestrial organic carbon records from the northwestern Pacific (Hasegawa, 1997).

5.3. Stratigraphic significance of $\delta^{13}C$ fluctuations

The marked positive $\delta^{13}C$ excursion in the Sawpit Gully sections occurs within an interval that is very conspicuously barren of macrofossils (ZBM hereafter: the upper part of the *Mrr* Zone below the *Cremnoceramus bicorrugatus matamuus* Zone) (Fig. 14C, D). For three reasons, this isotope excursion is correlated here with the globally well-known carbon isotope excursion across the Cenomanian/Turonian boundary (C/T CIE). First, dinoflagellate biostratigraphic data from the Mangaotane A and Sawpit Gully sections support our interpretation that the Cenomanian/Turonian boundary is located within the ZBM (Fig. 14). Secondly, the pattern of $\delta^{13}C$ variation within the ZBM in southern Sawpit Gully section is remarkably similar to the C/T CIE reported from Eastbourne (UK), Pueblo (Colorado, USA), Guerrero (Mexico), and Tappu (Hokkaido, Japan) (Fig. 15A–C, E). At the onset of the C/T

CIE, a positive shift of $\delta^{13}C$ values is more rapid than the subsequent recovery phase. A negative "trough" just above the onset, is followed by a maximum, a stable phase, and lastly a gradual shift back to the background level; this pattern is observed in all the C/T CIE sections shown in Fig. 15. Thirdly, the magnitude of the C/T CIE recorded by terrestrial organic carbon elsewhere on the globe is known to be as large as 2–2.5‰ (Hasegawa, 1997; Gale et al., 2005; Hasegawa et al., 2010), and similar values are observed in the Sawpit Gully sections (Fig. 15D).

Adopting this correlation for this $\delta^{13}C$ excursion in the Sawpit Gully section, using the nomenclature for distinct positive "peaks" in the excursion as shown in Fig. 15, and by correlation with the global boundary stratotype for the base of the Turonian Stage (Kennedy et al., 2005), we suggest that the C/T boundary may lie between peaks B and C, at ~70 m ± 3 m in the southern section. If correct, this would place the boundary close to the top of the boundary interval defined by dinoflagellates. We stress that this correlation is consistent with existing data, but may be subject to revision as additional isotopic and biostratigraphic data come to light.

5.4. Interval of stable $\delta^{13}C$ values below C/T CIE

Carbon isotope values from ~100 to 215 m (P77189–P77225) in the Mangaotane A section are remarkably stable, although they increase slightly from -24.7 to -24.2‰ within the upper part of the *Mrh* Zone and the *Mrr* Zone below the inferred C/T CIE (Fig. 12B). This long-term pattern appears to trace the global middle to upper Cenomanian trend that is shown in the European reference curve below the C/T CIE (Jarvis et al., 2006). A comparable, increasing trend of $\delta^{13}C$ has not been recognized in the Glenburn section, probably because the sampled interval in this section is too short to detect the long-term trend. Because we could not detect the middle Cenomanian Event (MCE) in the upper *Mrh* and *Mrr* zones, it seems likely that the MCE is located within or below the middle part of the *Mrh* Zone. We have not evaluated $\delta^{13}C$ fluctuations below P77189 in the Mangaotane A section because of the problematic data discussed previously (samples P77181, 77184 and 77185) and the relatively wide sampling interval that could mask short-lived isotopic events.

5.5. Cenomanian bioevents in the high latitude South Pacific: a prelude to OAE2?

As described above, we have identified sedimentary sequences in New Zealand (NZ) that were deposited on the shelf and continental slope during OAE2. Even though OAE2 is known to mark an episode of environmental deterioration, macrofossils have been collected from this stratigraphic interval in many well-studied carbonate successions (Elder, 1989; Kennedy and Cobban, 1991; Gale et al., 2005). In contrast, no macrofossils have been observed in the otherwise richly fossiliferous NZ sections spanning the OAE2 interval. This observation apparently holds true for other sections in NZ that have not been examined here in detail (e.g., Lower Mata River and Kirk's Clearing sections, see Crampton, 1996; and the Te Waka Stream and Puketoro Stream sections, JSC unpublished data). Similar macrofossil-barren intervals have been described in the Japanese Oyubari (Hirano, 1995; Toshimitsu et al., 1995) and Tappu (Sekine et al., 1985; Asai and Hirano, 1990) sections of fore-arc basin settings. In Japan, however, such barren intervals are more restricted than in NZ (Nemoto and Hasegawa, 2011). An example of the Tappu section is shown in Fig. 15E: the highest occurrence of Cenomanian inoceramids is located at "peak A" of the C/T CIE and the lowest occurrence of Turonian inoceramid species is located just above "peak C". In this case, oxygen depletion was apparently not a causal factor in the macrofossil absence (Nemoto and Hasegawa, 2011).

The extended barren interval (ZBM) seems to be a distinctive feature of the NZ sections and indicates a unique environmental response to OAE2 in the high latitude South Pacific.

Recent studies have focused on a large volcanic pulse as a causal factor or “trigger” of OAE2, and evidence of the volcanic activity has been found just below the onset of the C/T CIE (Turgeon and Creaser, 2008). These authors estimated that the volcanic pulse was initiated approximately 23 kyr before the onset of the C/T CIE. In the NZ sections, the ZBM may have started significantly earlier than the inferred volcanic pulse. Assuming the duration of the C/T CIE (from the onset to “peak C”) as 500–540 kyr based on correlation with the Pueblo section (Sageman et al., 2006; Meyers et al., 2012), and assuming a constant sedimentation rate, the last occurrence of Cenomanian macrofossils in the NZ sections is very approximately >500 kyr prior to the onset of the C/T CIE. If this estimation is correct, the volcanic pulse discussed as a “trigger” of OAE2 was not a causal factor of the faunal deterioration of NZ sections. Environmental change in the shallow to bathyal range of the ocean in high latitudes of the South Pacific started much earlier than typical OAE2 onset. This implies that the causal mechanism(s) of OAE2 may be complex.

5.6. Oxic event during OAE2 in high latitude South Pacific

Another unique feature of the NZ sections deposited in bathyal settings is the presence of conspicuous red beds within the ZBM. In the Mangaotane sections, a thick red bed occupies the upper part of the ZBM (Fig. 14A, B), and alternating beds of red and grey or slightly greenish mudstone occur in the lower part of the ZBM. We infer a close association between the deposition or formation of red beds and macrobenthic ecology (Figs. 3, 4). Based on correlations between the Mangaotane A and Sawpit Gully sections (Fig. 14), we also infer that the alternating, thin red beds are correlated with the lower part of the C/T CIE and the thick red bed is correlated with the upper part or with the interval just above the main part of the C/T CIE. The entire red bed interval, including the alternating beds, apparently spans much of the C/T CIE. Thus, in NZ, the situation is apparently different from that observed in many other regions of the globe, where the C/T CIE is commonly associated with black shales deposited during OAE2 (e.g., Wang et al. 2011 and references therein) and red beds overlie the C/T CIE.

In terms of organic characteristics, the red mudstone contrasts with grey mudstone above and below. The red mudstone has: (1) a low concentration of terrestrial kerogens (P77234, P77235); (2) a comparatively high contribution of fusinite to kerogen composition and a correspondingly low proportion of semifusinite and vitrinites (the concentration of fusinite itself does not increase); (3) an absence or very low abundance of dinoflagellates. These observations, and the red colour itself, are consistent with the existence of strongly oxic conditions at the depositional site, such that the majority of organic matter was oxidized and eliminated from the sediment, leaving only highly resistant fusinite. Since the Sawpit Gully section, inferred to have been deposited at shelf depths, does not show a decrease in TOC_{cf} in the ZBM (Fig. 9), this "oxic event" appears to have been restricted to intermediate water depths.

It is worth noting that evidence for benthic oxygenation during deposition of the ZBM in the NZ sections and in the Japanese Tappu section, discussed above, suggests that the presence or elimination of the benthic macrofauna was not a simple consequence of water column anoxia (e.g., Ifrim et al., 2011), but must have had more complex and as-yet unknown causes. The presence of macrofossils within stratigraphically lower, thin red beds in the Mangaotane A section, just below the *Mrh/Mrr* zone boundary (~120 m; Fig. 3), suggests that absence of calcareous macrofauna from the ZBM is not a simple taphonomic signal related in some way to the formation of red beds. Likewise, the expression of the ZBM in the "normal" siltstone and sandstone of the Sawpit Gully sections also indicates that the absence of macrofauna was not a simple, direct consequence of the formation of coloured beds.

Although this paper is not the place to speculate on palaeoceanographic conditions that resulted in the stratigraphic patterns observed in NZ, we note that a number of authors have postulated that one key area of deep water formation and ocean ventilation during the mid-Cretaceous may have been along the Antarctic margin between Australia and South America, i.e., in the New Zealand region (Hay, 2009, and references therein). Our findings are certainly consistent with such a model. Finally, we note that our findings are also commensurate with the closing comment by Hay (2009, p. 267), who suggested that ocean-wide anoxia during the mid-Cretaceous should not necessarily be expected in the Pacific Ocean basin except at specific sites of local upwelling.

6. Conclusions

Based on dinoflagellate biostratigraphic data and carbon isotope stratigraphy, we identify the C/T boundary and C/T CIE within the uppermost part of the New Zealand Arowhanan Stage, in an interval that is barren of macrofossils. Environmental changes associated with OAE2 may have been initiated earlier in New Zealand than in Europe and the northwestern Pacific. Oxic intermediate water produced within the southernmost Pacific during OAE2 appears to be a plausible explanation for red-bed development. A surplus of oxygen that compensated for the CO_2 removed and deposited as organic matter during OAE2, and related cooling (Voigt et al., 2006; Forster et al., 2007), could have provided the necessary conditions for production of such a water mass.

Acknowledgments

We have greatly appreciated the constructive suggestions of Dr. C. Hollis and an anonymous reviewer. We are grateful for the assistance of Dr. Y. Tominaga and graduate students of Hasegawa’s laboratory at Kanazawa University, and the technical staff of the GNS Rafter Isotope Laboratory. This study was supported financially by Grants-in-Aid for

Scientific Research (20403016, 20340144, 23340158, 24403012) from the JSPS and by Presidential Grant of Kanazawa University (all awarded to T. Hasegawa). J. Crampton and P. Schiøler acknowledge funding from the NZ Foundation for Research, Science and Technology, research contracts C05X0701 and C05X0905 to GNS Science.

References

Arthur, M.A., Dean, W.E., Pratt, L.M., 1988. Geochemical and climatic effects of increased marine organic carbon burial at the Cenomanian/Turonian boundary. Nature 335, 714–717.

Arthur, M.A., Premoli Silva, I., 1982. Development of widespread organic carbon-rich strata in the Mediterranean Tethys. In: Schlanger, S.O., Cita, M.B. (Eds.), Nature and Origin of Cretaceous Carbon-rich Facies. Academic Press, New York, NY, pp. 7–54.

Arthur, M.A., Schlanger, S.O., Jenkyns, H.C., 1987. The Cenomanian–Turonian Oceanic Anoxic Event, II. Palaeoceanographic controls on organic-matter production and preservation. In: Brooks, J.M., Fleet, A.J. (Eds.), Marine Petroleum Source Rocks. Geological Society, London, Special Publication, 26, pp. 401–420.

Asai, A., Hirano, H., 1990. Stratigraphy of Upper Cretaceous in the Obira area, northwestern Hokkaiko. Gakujutsu Kenkyu, School of Education, Waseda University, Biology and Geology Series 39, 37–50.

Barclay, R.S., McElwain, J.C., Sageman, B.B., 2010. Carbon sequestration activated by a volcanic CO_2 pulse during Ocean Anoxic Event 2. Nature Geoscience 3, 205–208.

Barnes, C., Hallam, A., Kaljo, D., Kauffman, E.G., Walliser, O.H., 1995. Global event stratigraphy. In: Walliser, O.H. (Ed.), Global Events and Event Stratigraphy in the Phanerozoic: Results of International Interdisciplinary Cooperation in the IGCP

Project 216 "Global Biological Events in Earth History". Springer, Berlin, pp. 319–333.

Batten, D.J., 1999. Small palynomorphs. In: Jones, T.P., Rowe, N.P. (Eds.), Fossil Plants and Spores: Modern Techniques. Geological Society, London, pp. 15–19.

Bustin, R.M., Cameron, A.R., Grieve, D.A., Kalkreuth, W.D., 1983. Coal petrology, its principles, methods, and applications. Geological Association of Canada, Short Course Notes 3, 230–233.

Clarke, L.J., Jenkyns, H.C., 1999. New oxygen isotope evidence for long-term Cretaceous climatic change in the Southern Hemisphere. Geology 27, 699–702.

Cooper, R.A., 2004. The New Zealand geological timescale. Institute of Geological and Nuclear Sciences, Monograph 22, 284 pp.

Costa, L., Davey, R.J., 1992. Dinoflagellate cysts of the Cretaceous System. In: Powell, A.J. (Ed.), A Stratigraphic Index of Dinoflagellate Cysts. Chapman and Hall, London, pp. 99–153.

Courtinat, B., 1993. The significance of palynofacies fluctuations in the Greenhorn Formation (Cenomanian–Turonian) of the Western Interior Basin, USA. Marine Micropaleontology 21, 249–257.

Crampton, J.S., 1996. Inoceramid bivalves from the Late Cretaceous of New Zealand. Institute of Geological and Nuclear Sciences, Monograph 14, iv + 188 pp.

Crampton, J.S., 1997. The Cretaceous stratigraphy of the southern Hawke's Bay – Wairarapa region. Institute of Geological and Nuclear Sciences, Science Report 97/08, iv + 92 pp.

Crampton, J.S., Laird, M., Nicol, A., Hollis, C., Van Dissen, R., 1998. Field trip 6; geology at the northern end of the Clarence valley, Marlborough: a complete record spanning the Rangitata to Kaikoura orogenies. Geological Society of New Zealand, Miscellaneous Publication 101B, 1–35.

Crampton, J.S., Laird, M., Nicol, A., Townsend, D., Van Dissen, R., 2003. Palinspastic reconstructions of southeastern Marlborough, New Zealand, for mid-Cretaceous–Eocene times. New Zealand Journal of Geology and Geophysics 46, 153–175.

Crampton, J.S., Raine, I., Strong, P., Wilson, G., 2001. Integrated biostratigraphy of the Raukumara Series (Cenomanian–Coniacian) at Mangaotane Stream, Raukumara Peninsula, New Zealand. New Zealand Journal of Geology and Geophysics 44, 365–389.

Crampton, J.S., Tulloch, A.J., Wilson, G.J., Ramezani, J., Speden, I.G., 2004. Definition, age, and correlation of the Clarence Series stages in New Zealand (late Early to early Late Cretaceous). New Zealand Journal of Geology and Geophysics 47, 1–19.

Dodsworth, P., 2000. Trans-Atlantic dinoflagellate cyst stratigraphy across the Cenomanian–Turonian (Cretaceous) stage boundary. Journal of Micropalaeontology 19, 69–84.

Dodsworth, P., 2004. The distribution of dinoflagellate cysts across a Late Cenomanian carbon isotope ($\delta^{13}C$) anomaly in the Pulawi borehole, central Poland. Journal of Micropalaeontology 23, 77–80.

Elder, W.P., 1989. Molluscan extinction patterns across the Cenomanian–Turonian stage boundary in the western interior of the United States. Paleobiology 15, 299–320.

Erlick, M., Molina-Garza, R., Duncan, R., Snow, L., 2009. C-isotope stratigraphy and paleoenvironmental changes across OAE2 (mid-Cretaceous) from shallow-water platform carbonates of southern Mexico. Earth and Planetary Science Letters 277, 295–306.

Espitalie, J., Deroo, G., Marquis, F., 1985. Rock-Eval Pyrolysis and its applications. Part two. Revue de l' Institut Français du Pétrole 40, 755–784. (In French)

Fensome, R.A., Lentin, J.K., Williams, G.L., 2004. The Lentin and Williams index of fossil dinoflagellates, 2004 edition. American Association of Stratigraphic Palynologists, Contributions Series 42, 909 pp.

Fensome, R.A., Williams, G.L., MacRae, R.A., 2009. Late Cretaceous and Cenozoic fossil dinoflagellates and other palynomorphs from the Scotian Margin, offshore eastern Canada. Journal of Systematic Palaeontology 7, 1–79.

Field, B.D., Uruski, C., 1997. Cretaceous–Cenozoic geology and petroleum systems of the East Coast region, New Zealand. Institute of Geological and Nuclear Sciences, Monograph 13, 244 pp. + enclosures.

Fitzpatrick, M.E.J., 1995. Dinoflagellate cyst biostratigraphy of the Turonian (Upper Cretaceous) of southern England. Cretaceous Research 16, 757–791.

Forster, A., Kuypers, M.M.M., Turgeon, S.C., Brumsack, H.-J., Petrizzo, M.R., Sinninghe Damsté, J.S., 2008. The Cenomanian/Turonian oceanic anoxic event in the South Atlantic: new insights from a geochemical study of DSDP Site 530A. Palaeogeography, Palaeoclimatology, Palaeoecology 267, 256–283.

Forster, A., Schouten, S., Moriya, K., Wilson, P.A., Sinninghe Damste J.S., 2007. Tropical warming and intermittent cooling during the Cenomanian/Turonian oceanic anoxic event 2: sea surface temperature records from the equatorial Atlantic. Paleoceanography 22, PA1219, 1211–1214.

Gale, A.S., Kennedy, W.J., Voigt, S., Walaszczyk, I., 2005. Stratigraphy of the Upper Cenomanian–Lower Turonian Chalk succession at Eastbourne, Sussex, UK: ammonites, inoceramid bivalves and stable carbon isotopes. Cretaceous Research 26, 460–487.

Harries, P.J., Little, C.T.S., 1999. The early Toarcian (Early Jurassic) and the Cenomanian–Turonian (Late Cretaceous) mass extinctions: similarities and contrasts. Palaeogeography, Palaeoclimatology, Palaeoecology 154, 39–66.

Hart, M.B., Dodsworth, D., Duane, A.M., 1993. The Late Cenomanian event in eastern England. Cretaceous Research 14, 495–508.

Hasegawa, T., 1997. Cenomanian–Turonian carbon isotope events recorded in terrestrial organic matter from northern Japan. Palaeogeography, Palaeoclimatology, Palaeoecology 130, 251–273.

Hasegawa, T., 2001. Predominance of terrigenous organic matter in Cretaceous marine fore-arc sediments, Japan and Far East Russia. International Journal of Coal Geology 47, 207–221.

Hasegawa, T., Saito, T., 1993. Global synchroneity of a positive carbon isotope excursion at the Cenomanian/Turonian boundary: validation by calcareous microfossil biostratigraphy of the Yezo Group, Hokkaido, Japan. Island Arc 2, 181–191.

Hasegawa, T., Seo, S., Moriya, K., Tominaga, Y., Nemoto, T., Naruse, T., 2010. High resolution carbon isotope stratigraphy across the Cenomanian/Turonian boundary in the Tappu area, Hokkaido, Japan: correlation with world reference sections. Science Reports of Kanazawa University 54, 49–62.

Hay, W.W., 2009. Cretaceous oceans and ocean modelling. SEPM Special Publication 91, 243–271.

Hay, W.W., DeConto, R.M., Wold, C.N., Wilson, K.M., Voigt, S., Schulz, M., Wold, A.R., Dullo, W.-C., Ronov, A.B., Balukhovsky, A.N., Soding, E., 1999. Alternative global Cretaceous paleogeography. In: Barrera, E., Johnson, C.C. (Eds.), Evolution of the Cretaceous Ocean-Climate System. Geological Society of America, Boulder, CO, pp. 1–47.

Hayes, J.M., 1993. Factors controlling ^{13}C contents of sedimentary organic compounds: principles and evidence. Marine Geology 113, 111–125.

Helby, R., Morgan, R., Partridge, A.D., 1987. A palynological zonation of the Australian Mesozoic. Association of Australasian Palaeontologists, Memoir 4, 1–94.

Hikuroa, D., Crampton, J., Field, B., Schiøler, P., 2009. Upper Cretaceous oceanic red beds in New Zealand. SEPM Special Publication 91, 145–150.

Hirano, H., 1995. Correlation of the Cenomanian/Turonian boundary between Japan and Western Interior of the United States in relation with oceanic anoxic event. Journal of the Geological Society of Japan 101, 13–18.

Hollis, C.J., Beu, A.G., Crampton, J.S., Jones, C.M., Crundwell, M.P., Morgans, H.E.G., Raine, J.I., Boyes, A.F., 2010. Calibration of the New Zealand Cretaceous–Cenozoic timescale to GTS2004. GNS Science Report 2010/43, 20 pp.

Hu, X., Wang, C., Scott, R.W., Wagreich, M., Jansa, L., 2009. Cretaceous oceanic red beds: stratigraphy, composition, origins, and paleoceanographic and paleoclimatic significance. SEPM Special Publication 91, 13–33.

Ifrim, C., Götz, S., Stinnesbeck, W., 2011. Fluctuations of the oxygen minimum zone at the end of Oceanic Anoxic Event 2 reflected by benthic and planktic fossils. Geology 39, 1043–1046.

Isaac, M.J., Herzer, R.H., Brook, F.J., Hayward, B.W., 1994. Cretaceous and Cenozoic sedimentary basins of Northland, New Zealand. Institute of Geological and Nuclear Sciences, Monograph 8, 203 pp.

Jarvis, I., Gale, A.S., Jenkyns, H.C., Pearce, M.A., 2006. Secular variation in Late Cretaceous carbon isotopes: a new $\delta^{13}C$ carbonate reference curve for the Cenomanian–Campanian (99.6–70.6 Ma). Geological Magazine 143, 561–608.

Jarvis, I., Lignum, J.S., Gröcke, D.R., Jenkyns, H.C., Pearce, M.A., 2011. Black shale deposition, atmospheric CO_2 drawdown, and cooling during the Cenomanian/Turonian Oceanic Anoxic Event. Paleoceanography 26, PA3201, doi:10.1029/2010PA002081.

Jenkyns, H.C., Matthews, A., Tsikos, H., Erel, Y., 2007. Nitrate reduction, sulfate reduction, and sedimentary iron isotope evolution during the Cenomanian–Turonian oceanic anoxic event. Paleoceanography 22, PA3208, doi:10.1029/2006PA001355.

Keating, J.M., Spencer-Jones, M., Newham, S., 1992. The stratigraphical palynology of the Kotick Point and Whisky Bay formations, Gustav Group (Cretaceous), James Ross Island. Antarctic Science 4, 279–292.

Kennedy, W.J., Cobban, W.A., 1991. Stratigraphy and interregional correlation of the Cenomanian–Turonian transition in the Western Interior of the United States near Pueblo, Colorado, a potential boundary stratotype for the base of the Turonian Stage. Newsletters on Stratigraphy 24, 1–33.

Kennedy, W.J., Walaszczyk, I., Cobban, W.A., 2005. The Global Boundary Stratotype Section and Point for the base of the Turonian Stage of the Cretaceous: Pueblo, Colorado, U.S.A. Episodes 28, 93–104.

Killops, S., 1996. A geochemical perspective of oil generation in New Zealand basins, 1996 NZ Petroleum Conference, proceedings. Ministry of Commerce, Wellington, NZ, pp. 179–187.

Kolonic, S., Wagner, T., Forster, A., Sinninghe Damsté, J.S., Walsworth-Bell, B., Erba, E., Turgeon, S., Brumsack, H.-J., Hassane Chellai, E., Tsikos, H., Kuhnt, W., Kuypers, M.M.M., 2005. Black shale deposition on the northwest African shelf during the Cenomanian/Turonian oceanic anoxic event: climate coupling and global organic carbon burial. Paleoceanography 20, PA1006/1001–1018.

Kuhnt, W., Herbin, J.P., Thurow, J., Wiedmann, J., 1990. Distribution of Cenomanian–Turonian organic facies in the western Mediterranean and along the adjacent Atlantic margin. In: Huc, A.Y. (Ed.), Deposition of Organic Facies. American Association of Petroleum Geologists, Tulsa, OK, pp. 133–160.

Kuroda, J., Ogawa, N.O., Tanimizu, M., Coffin, M.F., Tokuyama, M.F., Kitazato, H., Ohcouchi, N., 2007. Contemporaneous massive subaerial volcanism and Late Cretaceous Oceanic Anoxic Event 2. Earth and Planetary Science Letters 256, 211–223.

Lee, J.M., Begg, J.G., 2002. Geology of the Wairarapa area. Institute of Geological and Nuclear Sciences 1:250000 Geological Map 11, 66 pp. + map.

Linnert, C., Mutterlose, J., Erbacher, J., 2010. Calcareous nannofossils of the Cenomanian/Turonian boundary interval from the Boreal Realm (Wunstorf, northwest Germany). Marine Micropaleontology 74, 38–58.

Marshall, K.L., Batten, D.J., 1988. Dinoflagellate cyst associations in Cenomanian–Turonian "Black Shale" sequences of northern Europe. Review of Palaeobotany and Palynology 54, 85–103.

Mazengarb, C., Speden, I.G., 2000. Geology of the Raukumara area. Institute of Geological and Nuclear Sciences 1:250000 geological map 6, 60 pp. + map.

Meyers, S.R., Siewert, S.E., Singer, B.S., Sageman, B.B., Condon, D.J., Obradovich, J.D., Jicha, B.R., Sawyer, D.A., 2012. Intercalibration of radioisotopic and astrochronologic time scales for the Cenomanian–Turonian boundary interval, Western Interior Basin, USA. Geology 40, 7–10.

Morgan, R., 1980. Palynostratigraphy of the Australian Early and middle Cretaceous. Memoirs of the Geological Survey of New South Wales; Palaeontology 18, 1-153.

Mort, H.P., Adatte, T., Follmi, K.B., Keller, G., Steinmann, P., Matera, V., Berner, Z., Stuben, D., 2007. Phosphorus and the roles of productivity and nutrient recycling during Oceanic Anoxic Event 2. Geology 35, 483–486.

Nemoto, T., Hasegawa, T., 2011. Submillennial resolution carbon isotope stratigraphy across the Oceanic Anoxic Event 2 horizon in the Tappu section, Hokkaido, Japan. Palaeogeography, Palaeoclimatology, Palaeoecology 309, 271–280.

Ogg, J., Ogg, G., Gradstein, F.M., 2008. The concise geologic time scale. Cambridge University Press, Cambridge, 177 pp.

Ohkouchi, N., Kawamura, K., Kajiwara, Y., Wada, E., Okada, M., Kanamatsu, T., Taira, A., 1999. Sulfur isotope records around Livello Bonarelli (northern Apennines, Italy) black shale at the Cenomanian–Turonian boundary. Geology 27, 535–538.

Omura, A.,Hoyanagi, K., 2004. Relationships between composition of organic matter, depositional environments, and sea-level changes in backarc basins, central Japan. Journal of Sedimentary Research 74, 620–630.

Otto-Bliesner, B.L., Brady, E.C., Shields, C., 2002. Late Cretaceous ocean; coupled simulations with the National Centre for Atmospheric Research climate system model. Journal of Geophysical Research – Atmospheres 107, 14.

Parente, M., Frijia, G., Di Lucia, M., Jenkyns, H.C., Woodfine, R.G., Baroncini, F., 2008. Stepwise extinction of larger foraminifers at the Cenomanian–Turonian boundary: a shallow-water perspective on nutrient fluctuations during Oceanic Anoxic Event 2 (Bonarelli event). Geology 36, 715–718.

Partridge, A.D., 2006. Jurassic–Early Cretaceous spore-pollen and dinocyst zonations for Australia. In: Monteil, E. (coord.), Australian Mesozoic and Cenozoic Palynology Zonations – Updated to the 2004 Geological Time Scale. Geoscience Australia, Record 2006/23 (wall chart), ISBN 1 921 236 05 1 (available at https://www.ga.gov.au/products/servlet/controller?event=GEOCAT_DETAILS&catno=64962).

Paul, C.R.C., Lamolda, M.A., Mitchell, S.F., Vaziri, M.R., Gorostidi, A., Marshall, J.D., 1999. The Cenomanian–Turonian boundary at Eastbourne (Sussex, UK): a proposed European reference section. Palaeogeography, Palaeoclimatology, Palaeoecology 150, 83–121.

Pearce, M.A., Jarvis, I., Swan, A.R.H., Murphy, A.M., Tocher, B.A., Edmunds, W.M., 2003. Integrating palynological and geochemical data in a new approach to palaeoecological studies: Upper Cretaceous and Banterwick Barn Chalk borehole, Berkshire, UK. Marine Micropaleontology 47, 271–306.

Pearce, M.A., Jarvis, I., Tocher, B.A., 2009. The Cenomanian–Turonian boundary event, OAE2, and palaeoenvironmental change in epicontinental seas: new insights from the dinocyst and geochemical records. Palaeogeography, Palaeoclimatology, Palaeoecology 280, 207–234.

Poulsen, C.J., Gendaszek, A.S., Jacob, R.L., 2003. Did the rifting of the Atlantic Ocean cause the Cretaceous thermal maximum? Geology 31, 115–118.

Pratt, L.M., Threlkeld, C.N., 1984. Stratigraphic significance of $^{13}C/^{12}C$ ratios in mid-Cretaceous rocks of the Western Interior, U.S.A. In: Stott, D.F., Glass, D.J. (Eds.), The Mesozoic of Middle North America. Canadian Society of Petroleum Geologists, Calgary, pp. 305–312.

Rattenbury, M.S., Townsend, D.B., Johnstone, M.R., 2006. Geology of the Kaikoura area. Institute of Geological and Nuclear Sciences 1:250000 Geological Map 13, 70 pp. + map.

Sageman, B.B., Meyers, S.R., Arthur, M.A., 2006. Orbital time scale and new C-isotope record for Cenomanian–Turonian boundary stratotype. Geology 34, 125–128.

Schlanger, S.O., Arthur, M.A., Jenkyns, H.C., Scholle, P.A., 1987. The Cenomanian–Turonian Oceanic Anoxic Event, I. Stratigraphy and distribution of organic carbon-rich beds and the marine delta ^{13}C excursion. In: Brooks, J.M., Fleet, A.J. (Eds.), Marine Petroleum Source Rocks. Geological Society, London, Special Publication 26 pp. 371–399.

Schlanger, S.O., Jenkyns, H.C., 1976. Cretaceous oceanic anoxic events: causes and consequences. Geologie en Mijnbouw 55, 179–184.

Sekine, H., Takagi, J., Hirano, H., 1985. Biostratigraphical study of the Upper Cretaceous of the north-east part of the Obira area, Hokkaido. Fossils [Tokyo] 38, 1–15.

Sepkoski, J.J., Raup, D., 1986. Periodicity in marine extinction events. In: Elliott, D.K. (Ed.), Dynamics of Extinction. Wiley, New York, NY, pp. 3–36.

Smith, A.B., Gale, A.S., Monks, N.E.A., 2001. Sea-level change and rock-record bias in the Cretaceous: a problem for extinction and biodiversity studies. Paleobiology 27, 241–253.

Snow, L.J., Duncan, R.A., Bralower, T.J., 2005. Trace element abundances in the Rock Canyon Anticline, Pueblo, Colorado, marine sedimentary section and their relationship to Caribbean plateau construction and Ocean Anoxic Event 2. Paleoceanography 20, 1–14.

Sutherland, R., 1999. Basement geology and tectonic development of the greater New Zealand region: an interpretation from regional magnetic data. Tectonophysics 308, 341–362.

Toshimitsu, S., Matsumoto, T., Noda, M., Nishida, T., Maiya, S., 1995. Towards an integrated mega-, micro- and magneto-stratigraphy of the Upper Cretaceous in Japan. Journal of the Geological Society of Japan 101, 19–29.

Turgeon, S.C., Creaser, R.A., 2008. Cretaceous Oceanic Anoxic Event 2 triggered by a massive magmatic episode. Nature 454, 323–326.

Tyson, R.V., 1995. Sedimentary Organic Matter: Organic Facies and Palynofacies. Chapman and Hall, London, 615 pp.

Uramoto, G.I., Abe, Y., Hirano, H., 2009. Carbon isotope fluctuations of terrestrial organic matter for the Upper Cretaceous (Cenomanian–Santonian) in the Obira area of Hokkaido, Japan. Geological Magazine 146, 761–744.

Van Bentum, E.C., Hetzel, A., Brumsack, H.-J., Forster, A., Reichart, G.-J., Sinninghe Damst, J.S., 2009. Reconstruction of water column anoxia in the equatorial Atlantic during the Cenomanian/Turonian oceanic anoxic event using biomarker and trace metal proxies. Palaeogeography, Palaeoclimatology, Palaeoecology 280, 489–498.

Voigt, S., Gale, A.S., Voigt, T., 2006. Sea-level change, carbon cycling and palaeoclimate during the Late Cenomanian of northwest Europe; an integrated palaeoenvironmental analysis. Cretaceous Research 27, 836–858.

Wang, C., Hu, X., Huang, Y., Wagreich, M., Scott, R., Hay, W., 2011. Cretaceous oceanic red beds as possible consequence of oceanic anoxic events. Sedimentary Geology 235, 27–37.

Wellman, H.W., 1959. Divisions of the New Zealand Cretaceous. Transactions of the Royal Society of New Zealand 87, 99–163.

Appendix.

Supplementary data associated with this article can be found, in the online version, at…….

Captions to figures and tables

Fig. 1. Map of central New Zealand showing key localities discussed in the text. Grey shading indicates distribution of Albian–Maastricthtian rocks.

Fig. 2. Simplified geological map of the Mangaotane Stream area, Raukumara Peninsula, showing the locations of the Mangaotane A and B sections. This map lies within 1:50000 topographical map series Topo50 sheet BE42. Geology after I.G. Speden (unpublished) and JSC (unpublished). Legend to this figure also applies to Figs. 6 and 8.

Fig. 3. Log of the Mangaotane A section; see Fig. 2 for location. In the TOC column, closed symbols indicate measurements derived from the peak area of the mass chromatograms and open symbols indicate measurements derived by Rock-Eval pyrolysis. The legend to this

figure also applies to Figs. 4, 7 and 9. Sample numbers in brackets indicate samples collected earlier that could not be located precisely in the log of 2005, although uncertainties are small (see text).

Fig. 4. Log of the Mangaotane B section; see Fig. 2 for location and Fig. 3 for legend. The section lies entirely within the *Magadiceramus rangatira rangatira* Zone (Arowhanan Stage) of the Karekare Formation. Note that TOC data are carbonate-free basis.

Fig. 5. Photograph of the base of the main red bed in the Mangaotane B section. The colour change ~ 2m above the seated figure is at 17.5 m on the log (Fig. 4). The outcrop is located at grid reference NZ Topo50 BE42 (Houpoto) 17527032 [NZMS 260 map series, sheet X16 (Motu), 27493167]

Fig. 6. Map of Horewai Point, Glenburn, Wairarapa, showing the location of the measured section. The map lies within 1:50000 topographical map series Topo50 sheet BQ35. See Fig. 2 for legend.

Fig. 7. Log of the Glenburn section; see Fig. 6 for location and Fig. 3 for legend. The section lies entirely within the Glenburn Formation. Note that TOC data are carbonate-free basis.

Fig. 8. Simplified geological map of the Coverham area, Marlborough, showing the location of the Sawpit Gully measured sections. The map lies within 1:50000 topographical map series Topo50 sheet BS28. See Fig. 2 for legend.

Fig. 9. Log of the Sawpit Gully sections; see Fig. 8 for location and Fig. 3 for legend. The section lies entirely within the Nidd Formation. Note that TOC data are carbonate-free basis.

Fig. 10. Selected dinoflagellates from the Mangaotane A section, Raukumara Peninsula, New Zealand. All specimens are at the same scale. Scale bar in A. Specimen names are followed by Fossil Record File number, preparation number (L-number), slide number and EF coordinates. A, *Kiokansium unituberculatum*, X16/f277, L22613/2, G44/0. B, *Sepispinula ambigua*, X16/f293, L22628/2, U27/0. C, *Lithosphaeridium siphoniphorum glabrum*, X16/f271, L22607/2, J29/3. D, *Ascodinium serratum*, X16/f270, L22606/2, E37/1. E, *Isabelidinium acuminatum*, X16/f295, L22630/2, P44/0. F, *Cyclonephelium compactum*, X16/f291, L22626/1, N28/0. G, *Cyclonephelium crassimarginatum*, X16/f292, L22627/2, P43/1. G, *Heterosphaeridium difficile*, X16/f302, L22637/2, N43/3. I, *Cyclonephelium clathromarginatum*, X16/f292, L22627/2, J42/0. J, *Hapsocysta peridictya*, X16/f280, L22616/3, E23/0. K, *Eurydinium saxoniense*, X16/f303, L22638/2, Y33/3. L, *Prolixosphaeridium conulum*, X16/f290, L22625/2, B28/0.

Fig. 11. Photomicrographs of organic matter. A, alginite (a dinoflagellate) under transmitted light, oil immersion, P77186. B, fusinite under reflected light, oil immersion, P77234. C, semifusinite under reflected light, oil immersion, P77199. D, vitrinite under reflected light, oil immersion, P77208. Note cell structure in semifusinite of C, demonstrating its origin from cellular lignins of terrestrial vascular plants.

Fig. 12. Long-term variation of A, carbonate-free based total organic carbon content (TOC_{cf}), and B, carbon isotope ratio ($\delta^{13}C$) through the Mangaotane A section. Note a trend of gradual increase of $\delta^{13}C$ up-section.

Fig. 13. Results of Rock Eval pyrolysis: cross plot of T_{max} and hydrogen index (HI) of selected samples from the Glenburn, Sawpit Gully and Mangaotane A sections. Also shown

are data from Hokkaido sections (Hasegawa, 1997; Uramoto et al., 2009) for comparison. Note that the data from the Sawpit Gully and Glenburn sections show remarkably similar distributions to those from the Oyubari and Tappu areas in Hokkaido.

Fig. 14. Correlation between the Mangaotane and Sawpit Gully sections on the basis of all available evidence. The interval above the highest occurrence of *Magadiceramus rangatira rangatira* (*Mrr*) and below the lowest occurrence of *Cremnoceramus bicorrugatus matamuus* (*Cbm*) lacks macrofossils and is indicated with pale shading as “Zone barren of macrofossils (ZBM)”. Red mudstone beds that are useful for local correlation are indicated with pale red shading. The interval containing the Cenomanian/Turonian boundary, as constrained using age-diagnostic dinoflagellate species in the Mangaotane A and Sawpit Gully sections, is indicated by dark shading. The stratigraphic intervals shown are as follows: Mangaotane section A, 172–255 m; Mangaotane section B, 0–37 m; Sawpit Gully, northern section, 0–45 m; Sawpit Gully, southern section, 0–92.5 m.

Fig. 15. Comparison between carbon isotope stratigraphy of A, carbonate carbon from Eastbourne, UK (Paul et al., 1999); B, marine organic carbon from Pueblo, Colorado, USA (Pratt and Threlkeld, 1984); C, carbonate carbon from Guerrero, Mexico (Elrick et al., 2009); D, terrestrial organic carbon from Sawpit Gully, new Zealand (this study); and E, terrestrial organic carbon from Tappu, Hokkaido, Japan (Hasegawa et al., 2010). An interval in the Tappu section that is barren of macrofossils is indicated by arrows in E (Sekine et al., 1985; Asai and Hirano, 1990). The highest occurrence of the Cenomanian inoceramid (*Inoceramus* sp. ex gr. *pennatulus*) and lowest occurrence of the Turonian inoceramid (*Inoceramus kamuy*) (Sekine et al., 1985) are also indicated. Correlations based on inflexions or peaks in the isotope record are indicated by broken lines.

Table 1. Distribution of key dinoflagellate taxa in the Mangaotane A section.

Table 2. Distribution of key dinoflagellate taxa in the Sawpit Gully sections.

Highlights

Cenomanian/Turonian boundary and carbon isotope excursion were identified in New Zealand, in an interval that is barren of macrofossils.

Environmental changes associated with OAE2 may have initiated earlier in New Zealand than in Europe and the northwestern Pacific.

Oxic intermediate water produced near the southernmost Pacific during OAE2 appears to be a plausible explanation for red bed development.

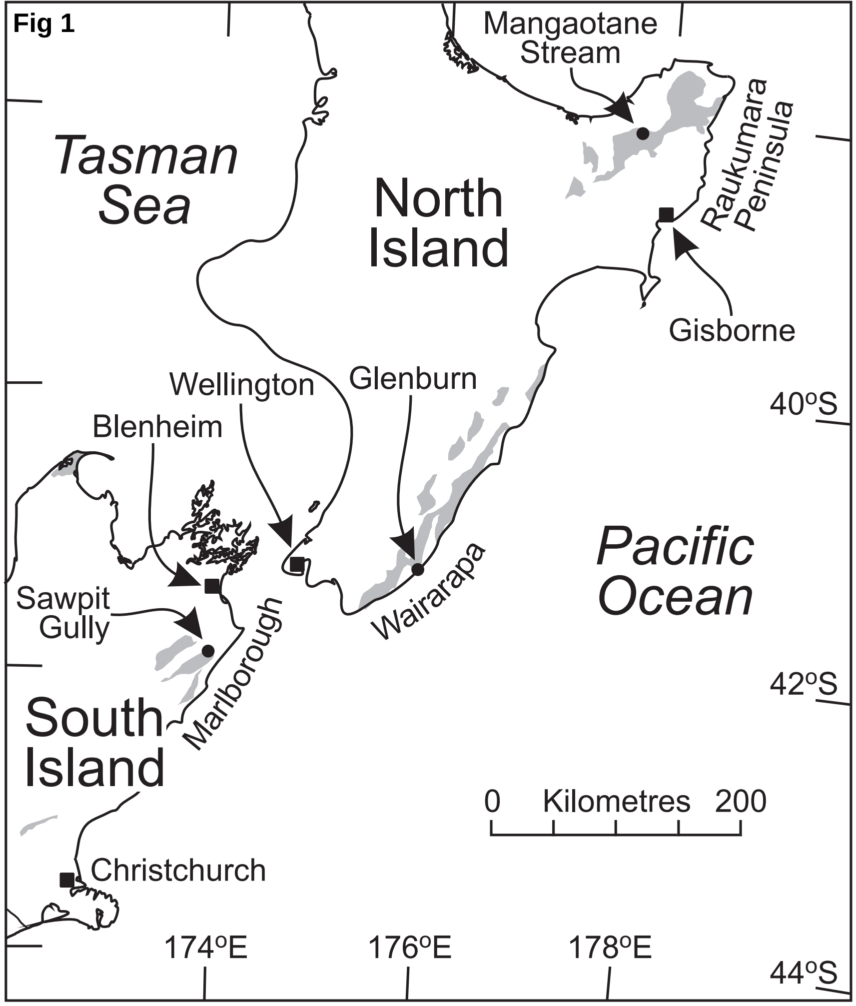

Fig. 1
Hasegawa et al.
One column

Figure 2

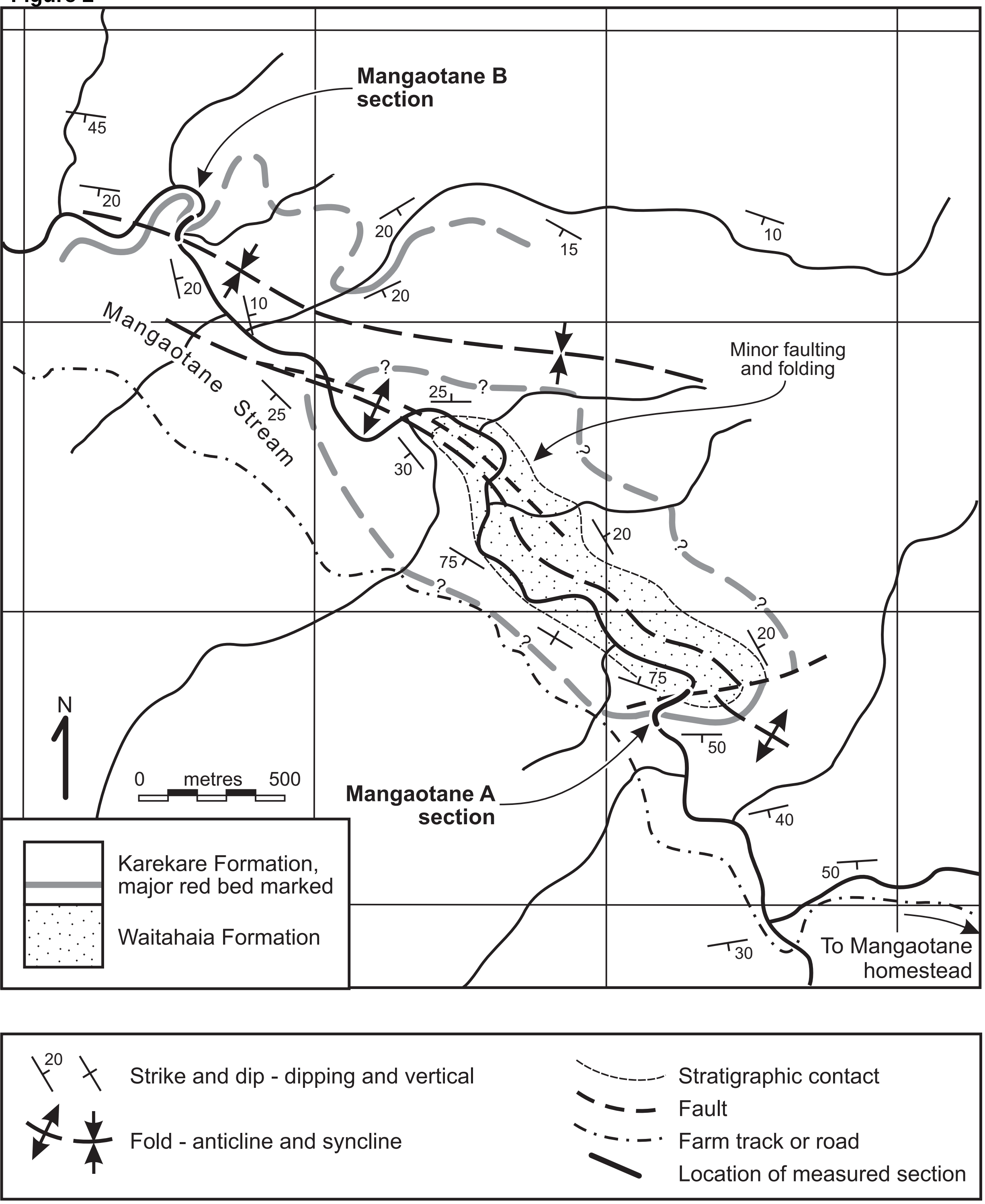

Fig. 2
Hasegawa et al.
1.5 column width

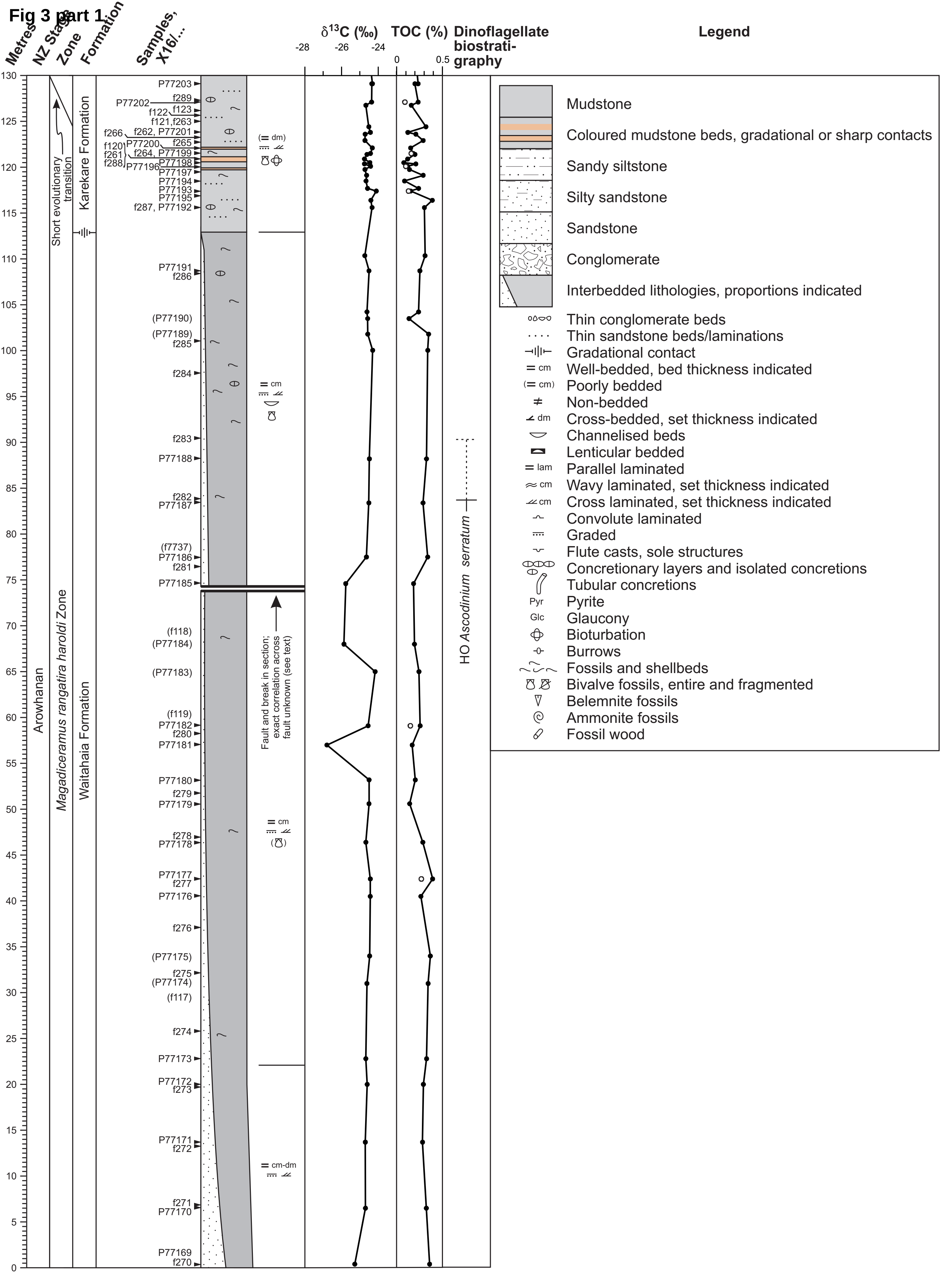

Fig. 3, part 1
Hasegawa et al.
2 column width, two facing pages

Figure 3 part 2 modified

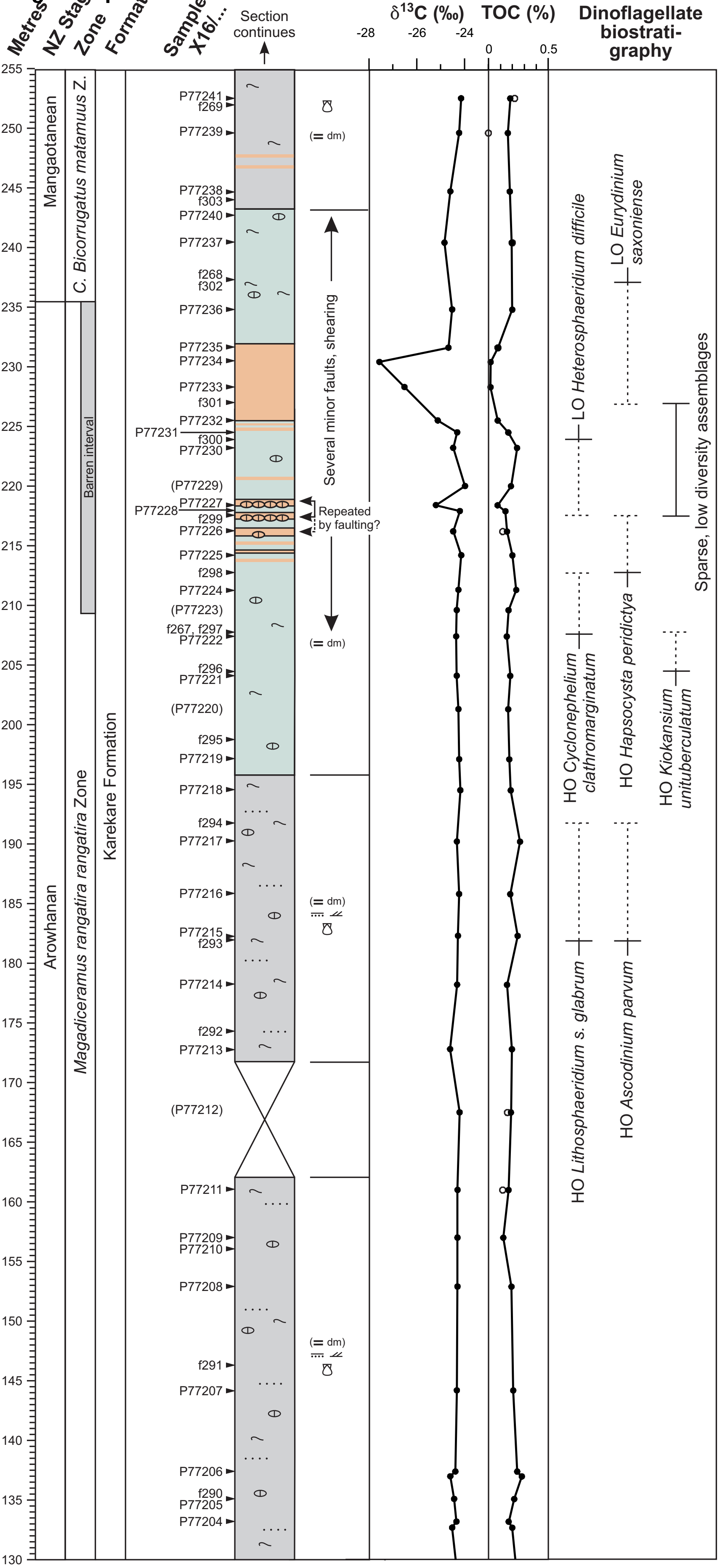

Fig. 3, part 2
Hasegawa et al.
1.5 column width, two facing pages

Figure 4

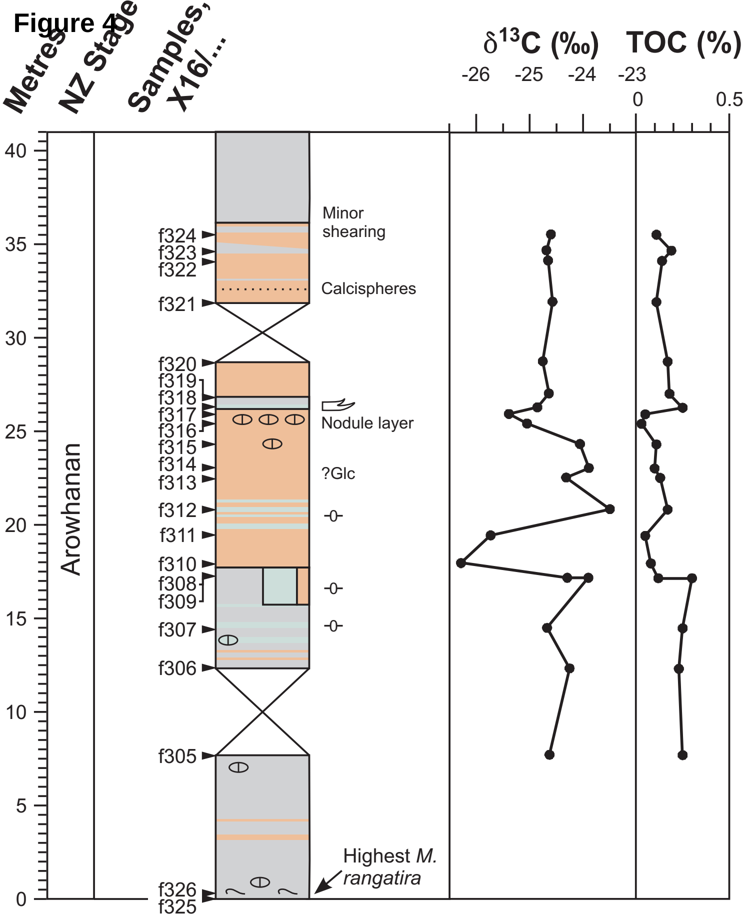

Fig. 4
Hasegawa et al.
1 column width

Figure 5
Click here to download high resolution image

Figure 6 modified

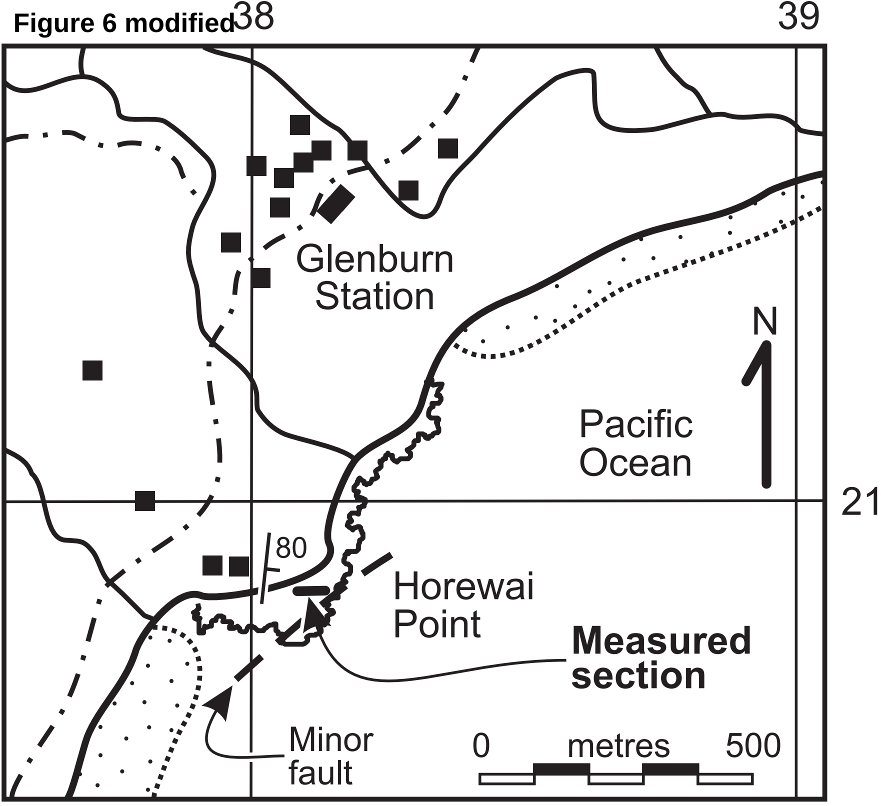

Fig. 6
Hasegawa et al.
1 column width

Figure 7

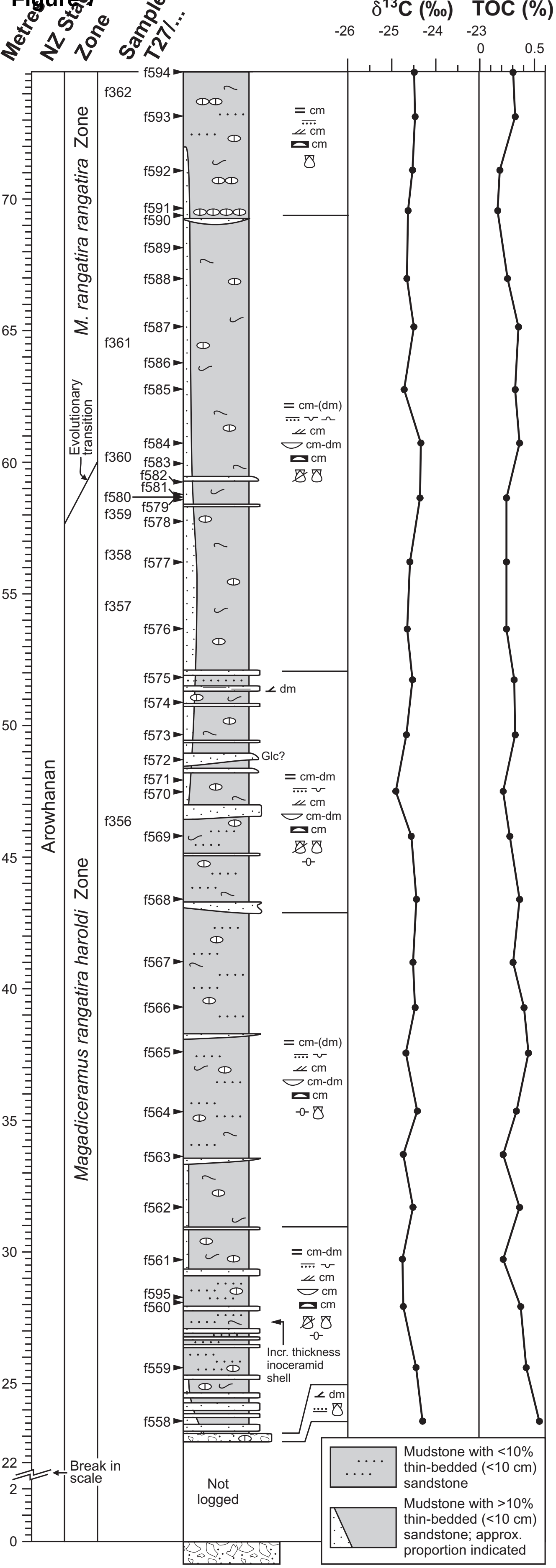

Fig. 7
Hasegawa et al.
1 column width

Figure 8

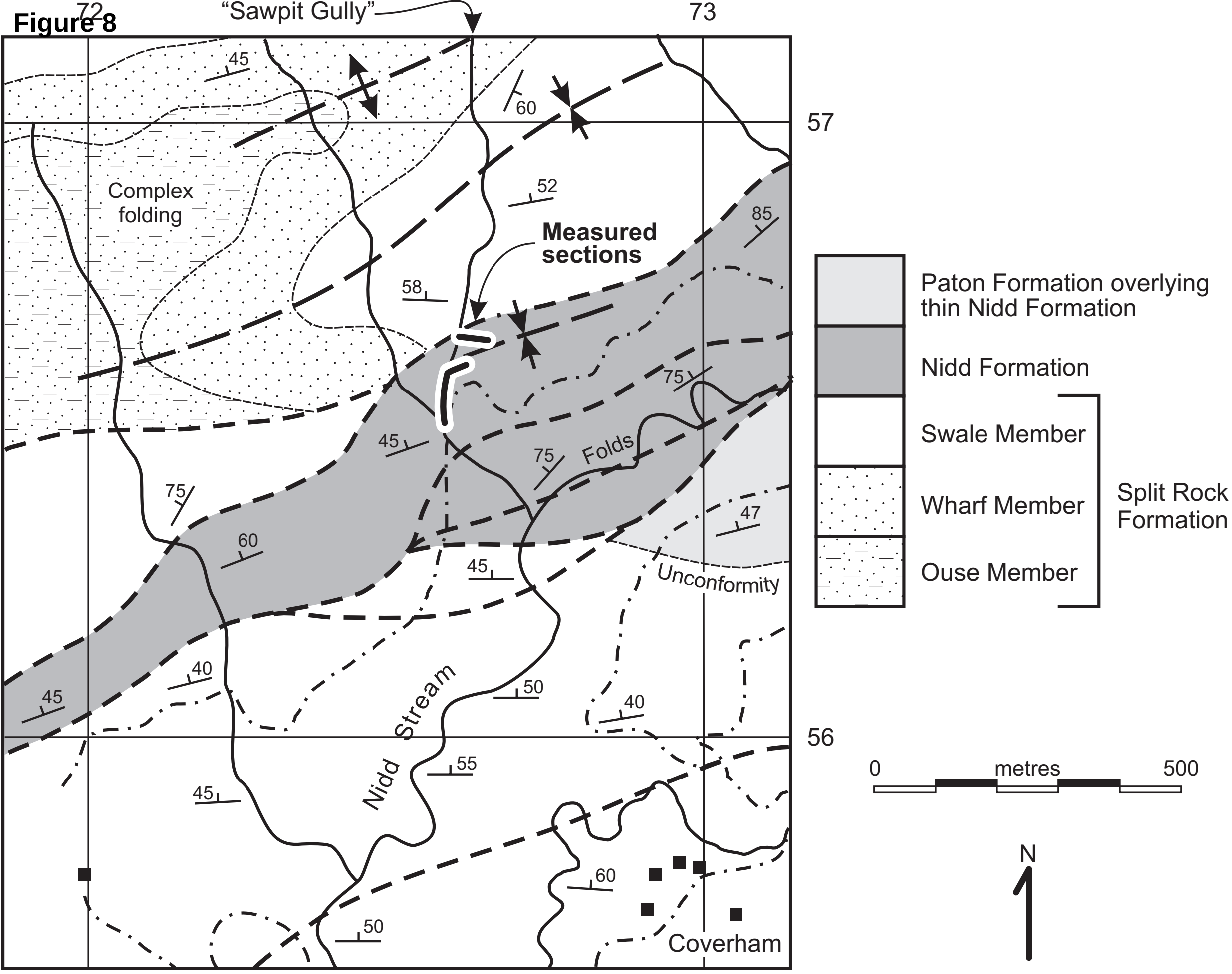

Fig. 8
Hasegawa et al.
1.5 column width

Fig 9 part 1

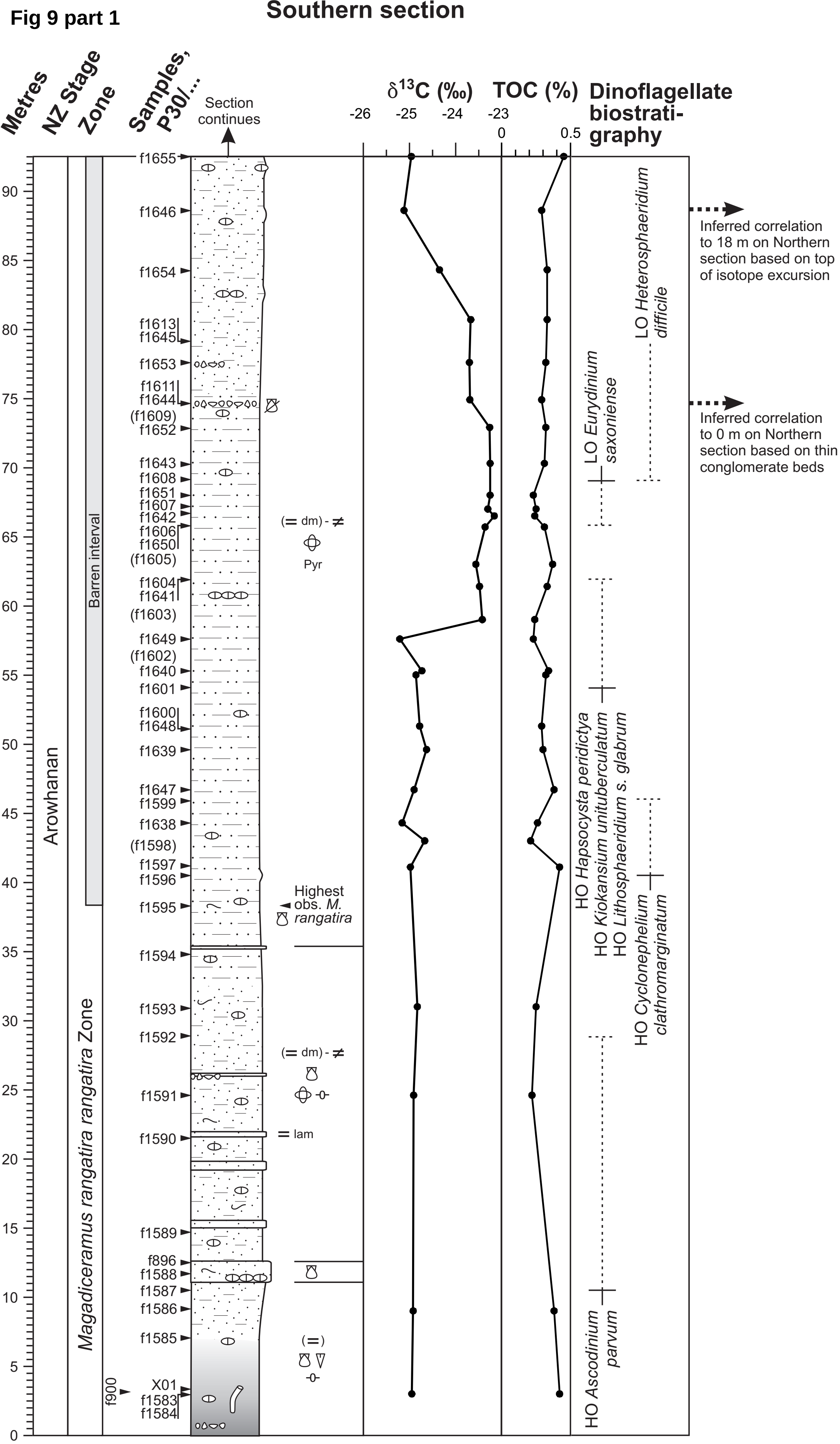

Fig. 9, part 1
Hasegawa et al.
1.5 column width

Fig 9 part 2

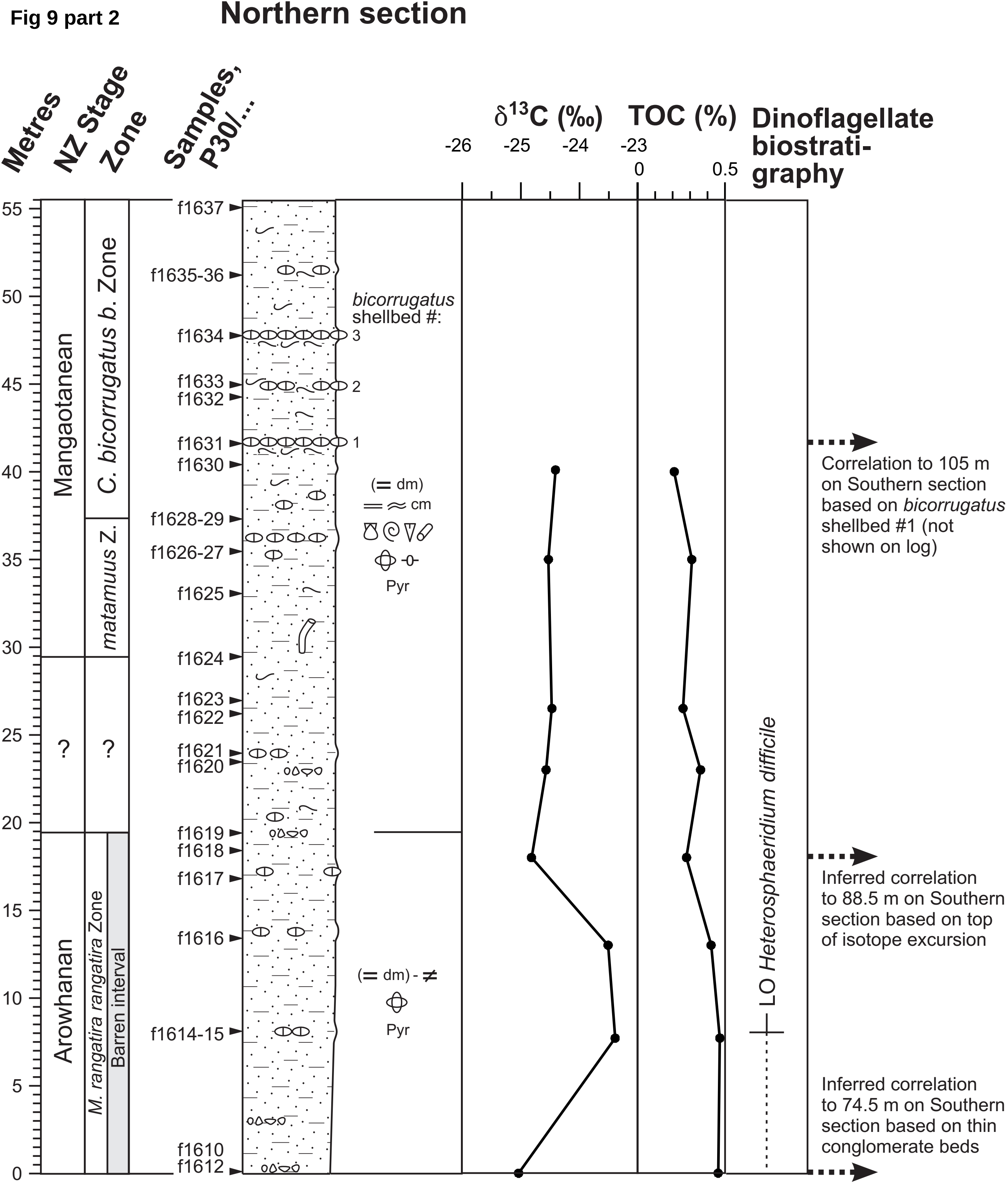

Fig. 9, part 2
Hasegawa et al.
1.5 column width

Fig 10
Click here to download high resolution image

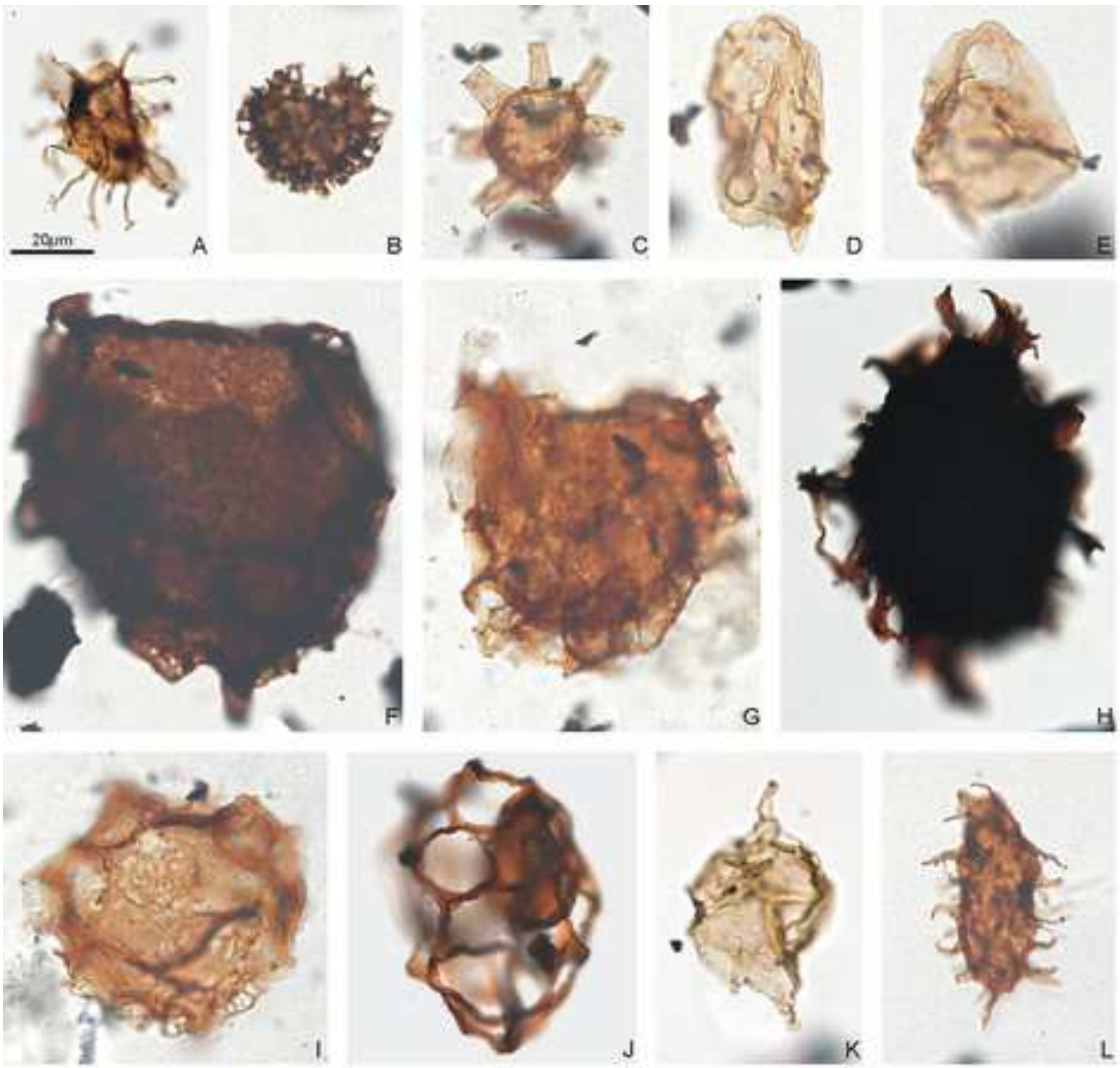

Figure 11

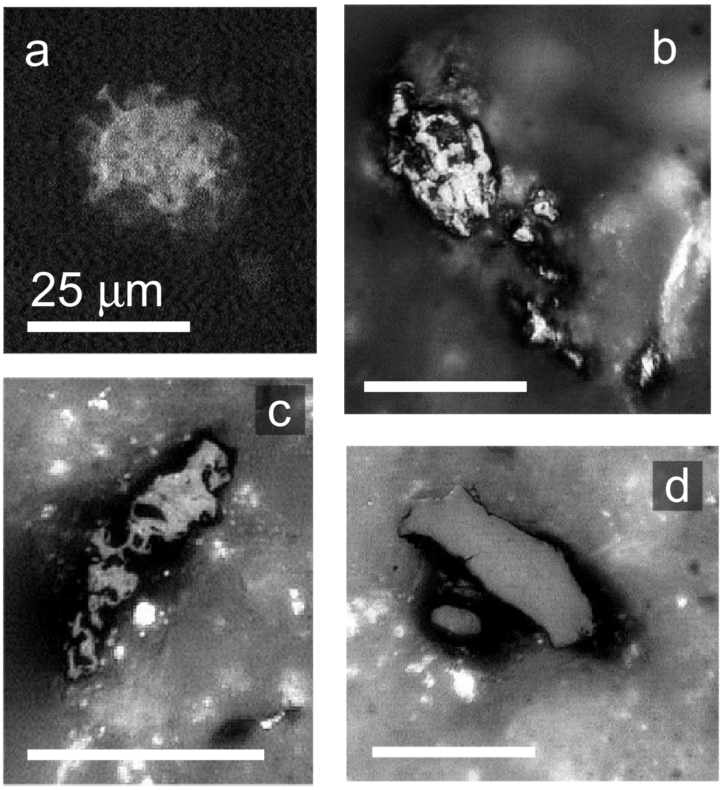

Fig. 11. Hasegawa et al.

Figure 12 jpg
Click here to download high resolution image

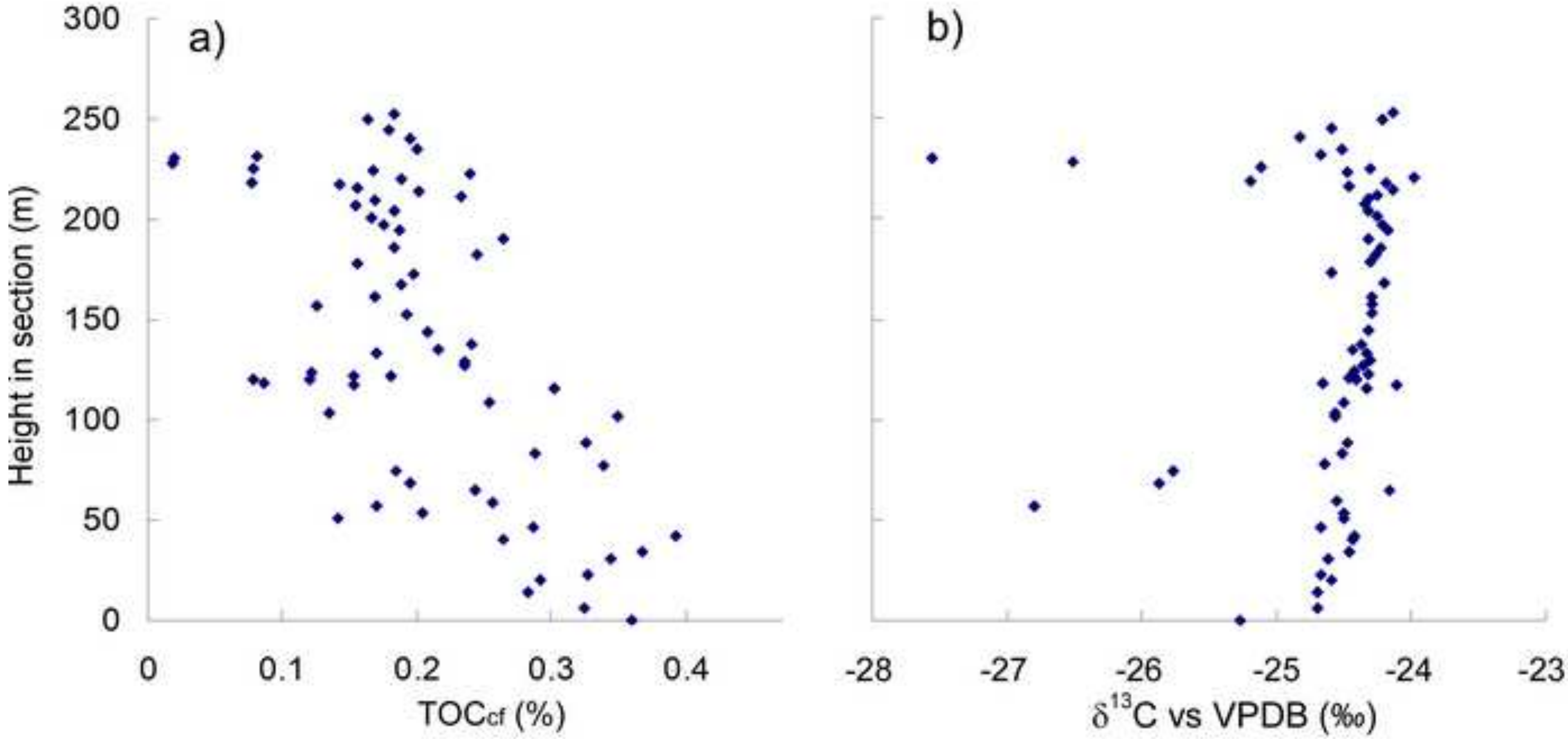

Figure 13

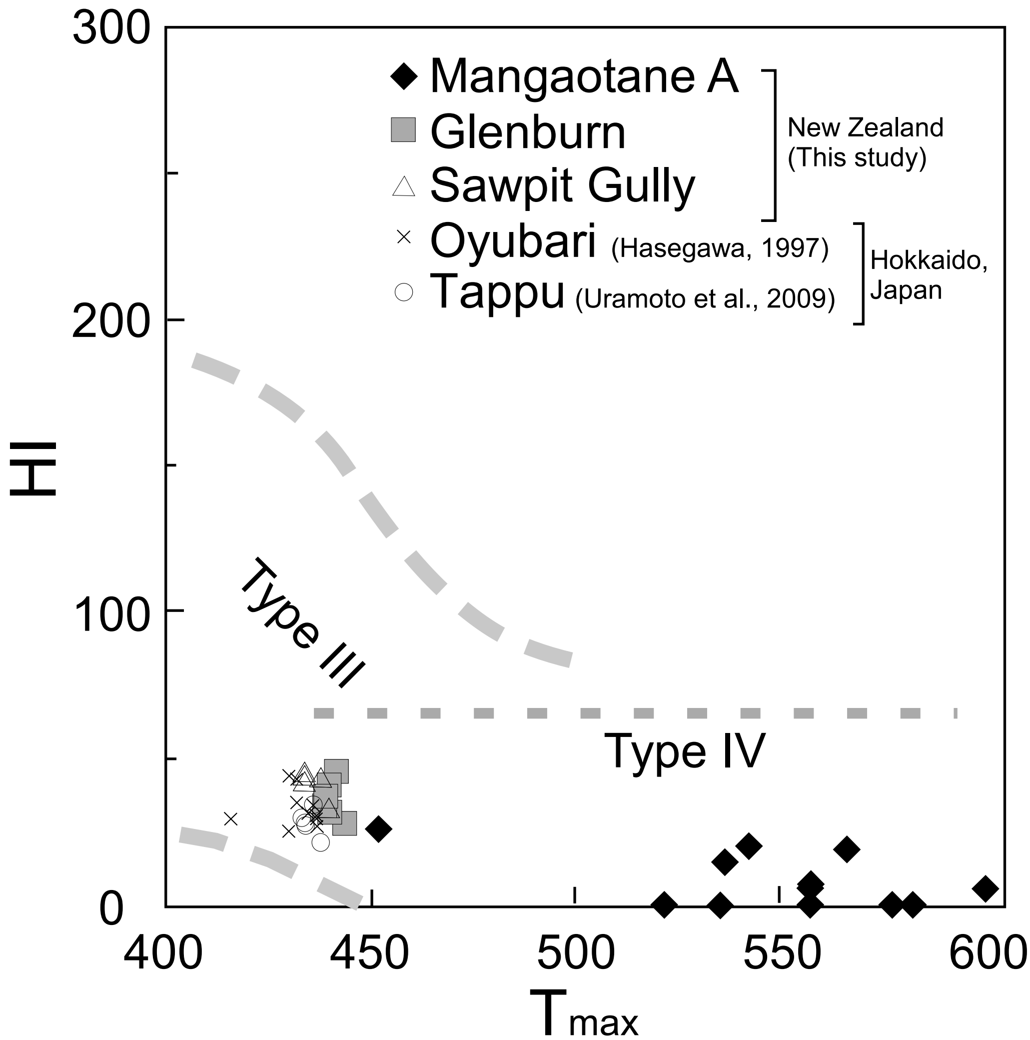

Mangaotane A
Glenburn
Sawpit Gully
New Zealand (This study)
Oyubari (Hasegawa, 1997)
Tappu (Uramoto et al., 2009)
Hokkaido, Japan
Type III
Type IV
HI
0
100
200
300
400
450
500
550
600
Tmax

Fig 14

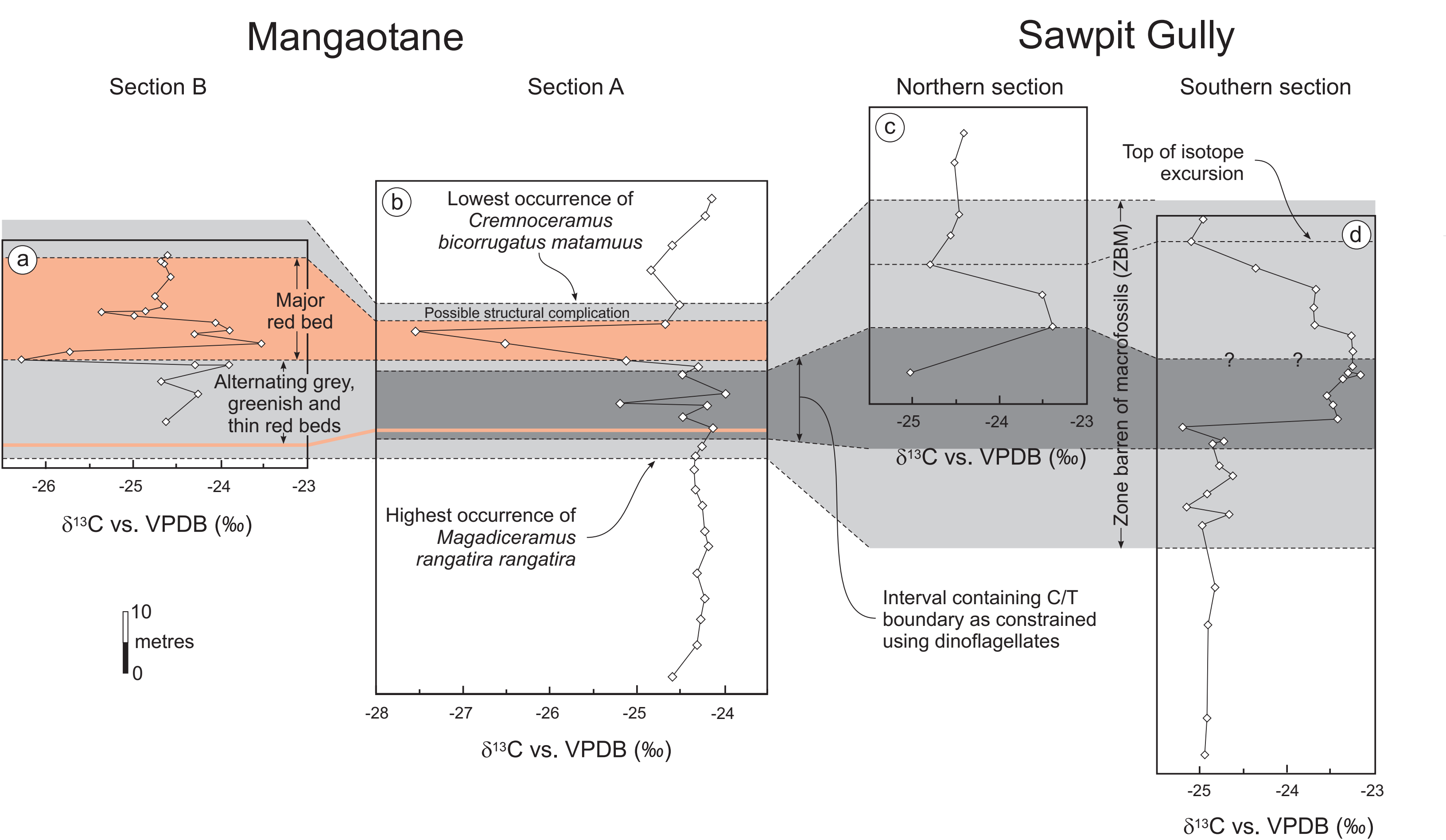

Mangaotane
Sawpit Gully
Section B
Section A
Northern section
Southern section
a
Major red bed
Alternating grey, greenish and thin red beds
-26
-25
-24
-23
δ13C vs. VPDB (‰)
10
metres
0
b
Lowest occurrence of Cremnoceramus bicorrugatus matamuus
Possible structural complication
Highest occurrence of Magadiceramus rangatira rangatira
-28
-27
-26
-25
-24
δ13C vs. VPDB (‰)
c
-25
-24
-23
δ13C vs. VPDB (‰)
Interval containing C/T boundary as constrained using dinoflagellates
Zone barren of macrofossils (ZBM)
Top of isotope excursion
d
?
?
-25
-24
-23
δ13C vs. VPDB (‰)

Figure 15 re-upload

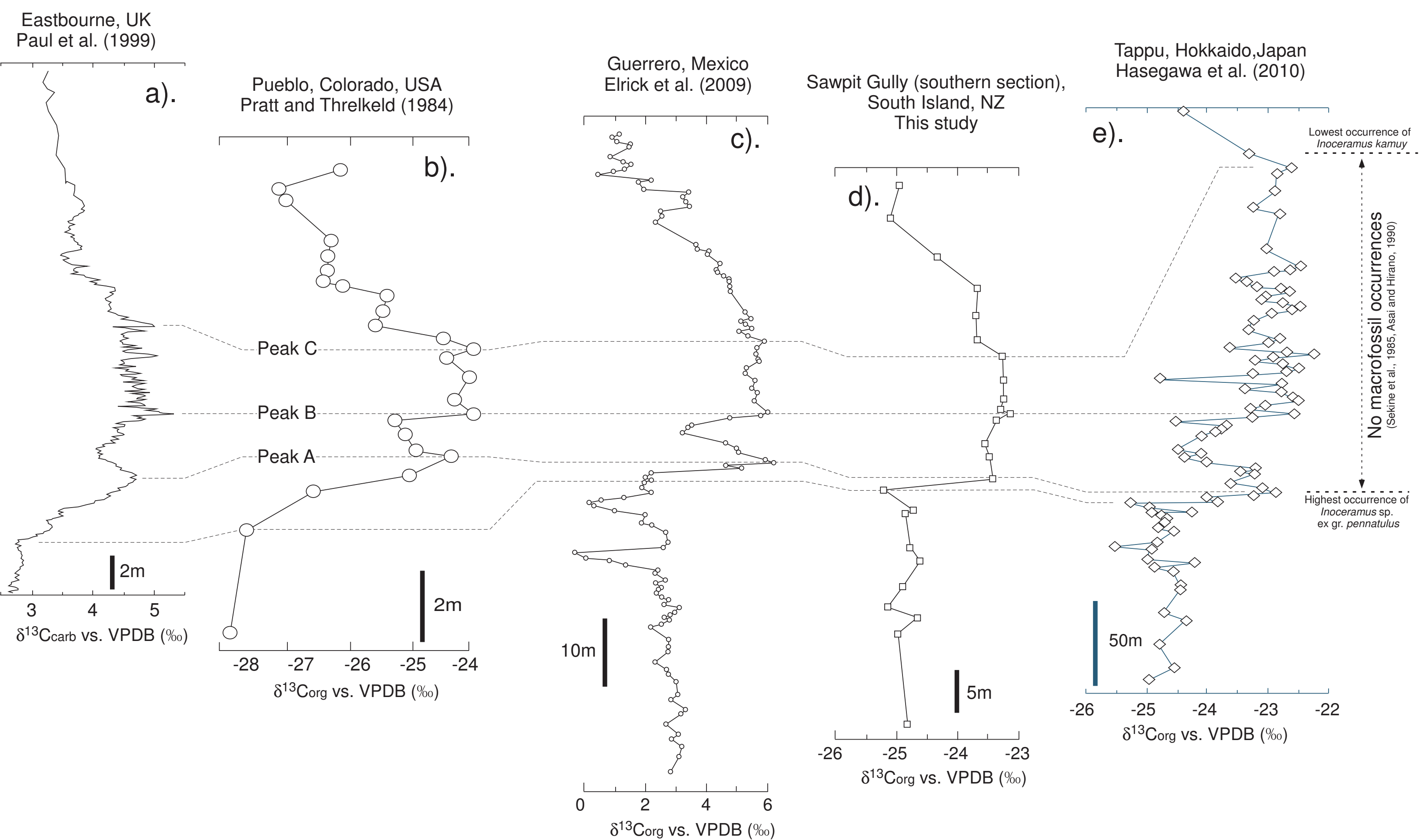

Table 1

Field number	Fossil Record File number, X16/f…	Palynological preparation number	Height (m)	*Ascodinium serratum*	*Lithosphaeridium s. glabrum*	*Ascodinium parvum*	*Kiokansium unituberculatum*	*Hapsocysta peridictya*	*Cyclonephelium compactum*	*Cyclonephelium clathromarginatum*	*Eurydinium saxoniense*	*Heterosphaeridium difficile*	Stage
MNGT-33	303	L22638	244.0						X		X	X	Turonian
MNGT-32	302	L22637	237.0						X		X	X	
MNGT-31	301	L22636	227.0										
MNGT-30	300	L22635	224.1				cf.		X			X	
MNGT-29	299	L22634	217.5	sample barren of dinoflagellates									
MNGT-28	298	L22633	212.7					X	X		X		Cenomanian
MNGT-27	297	L22632	207.6		cf.			X	X	X	X		
MNGT-26	296	L22631	204.4				X	X	X	X			
MNGT-25	295	L22630	198.7				cf.	X	X	X			
MNGT-24	294	L22629	191.7				X	X	X	X			
MNGT-23	293	L22628	181.9		X	X	X	X	X	X			
MNGT-22	292	L22627	174.3		cf.	X	X	X	X	X			
MNGT-21	291	L22626	146.4			cf.	X	X	X	X			
MNGT-20	290	L22625	135.0			X	X	X	X	X			
MNGT-19	289	L22624	127.3			X	X	X	X	X			
MNGT-18	288	L22623	120.9			X			X	X			
MNGT-17	287	L22622	115.5		X	X		X	X	X			
MNGT-16	286	L22621	108.4		X	X	X	X	X	X			
MNGT-15	284	L22620	97.5		X	X	X	X	X	X			
MNGT-14	283	L22619	90.4		X	X	X	X	X	X			
MNGT-13	282	L22618	83.7	X	X	X		X	X	X			
MNGT-12	281	L22617	76.4	X	X	X		X	X				
MNGT-11	280	L22616	58.2		X	X		X	X	X			
MNGT-10	279	L22615	51.7	X	X	X		X	X	X			
MNGT-9	278	L22614	46.9	X		X		X	X	X			
MNGT-8	277	L22613	42.4	X	X	X	X	X	X				
MNGT-7	276	L22612	37.0			X	cf.	X	X	X			
MNGT-6	275	L22611	32.1	X	X	X	cf.	X	X				
MNGT-5	274	L22610	25.8	X	X	X	X	X	X	X			
MNGT-4	273	L22609	19.7	X	X	X		X	X	X			
MNGT-3	272	L22608	13.2	X	X	X		X	X				
MNGT-2	271	L22607	6.8	X	X	X	X	X	X				
MNGT-1	270	L22606	0.4	X	X	X	X	X	X				

Table 2

Field number	Fossil Record File number, P30/f…	Palynological preparation number	Height (m)	*Ascodinium serratum*	*Lithosphaeridium s. glabrum*	*Ascodinium parvum*	*Kiokansium unituberculatum*	*Hapsocysta peridictya*	*Cyclonephelium clathromarginatum*	*Eurydinium saxoniense*	*Heterosphaeridium difficile*	Stage
SPG-25	1637	L23007	55.0									Turonian
SPG-24	1635	L23006	50.8									
SPG-23	1632	L23005	43.9									
SPG-22	1628	L23004	36.9							X		
SPG-21	1622	L23003	25.8							X		
SPG-20	1617	L23002	16.3							X		
SPG-19	1614	L23001	7.7							X	X	
SPG-17	1613	L22999	79.0									Cenomanian-Turonian
SPG-16	1611	L22998	75.0									
SPG-15	1608	L22997	69.1							X	cf.	
SPG-14	1606	L22996	65.7									
SPG-13	1604	L22995	61.9									
SPG-12	1601	L22994	54.1		X		X	X				Cenomanian
SPG-11	1600	L22993	51.1					X				
SPG-10	1599	L22992	46.0					X				
SPG-9	1596	L22991	40.5					X	X			
SPG-8	1594	L22990	34.8				cf.	X	X			
SPG-7	1592	L22989	28.9			cf.	X	X	X			
SPG-6	1590	L22988	21.5						X			
SPG-5	1589	L22987	14.7		cf.				X			
SPG-4	1588	L22986	11.7					X	X			
SPG-3	1587	L22985	10.5			X		X	X			
SPG-2	1585	L22984	7.0		X	X	X	X	X			
SPG-1	1583	L22983	3.0			X		X	X			